International Journal of Coal Geology 273 (2023) 104271

Contents lists available at ScienceDirect

International Journal of Coal Geology

journal homepage: www.elsevier.com/locate/coal

Cooper Basin REM gas shales after CO_2 storage or acid reactions: Metal mobilisation and methane accessible pore changes

J.K. Pearce [a,b,*], T. Blach [c], G.K.W. Dawson [b], G. Southam [b], D.J. Paterson [d], S.D. Golding [b], J. Bahadur [e], Y.B. Melnichenko [f,1], V. Rudolph [g]

[a] Centre for Natural Gas, University of Queensland, QLD, Australia
[b] School of Earth and Environmental Sciences, University of Queensland, QLD, Australia
[c] University of New South Wales, NSW, Australia
[d] Australian Synchrotron, ANSTO, Clayton, VIC, Australia
[e] Solid State Physics Division, Bhabha Atomic Research Centre, India
[f] Oakridge National Laboratory, USA
[g] School of Chemical Engineering, University of Queensland, QLD, Australia

ARTICLE INFO

Keywords:
SANS
Synchrotron XFM
Shales
CO_2 storage
Gas water rock reactions
Metal mobilisation

ABSTRACT

Shale - water - CO_2 reactions may occur during CO_2 geological storage, enhanced gas recovery, enhanced oil recovery, or supercritical CO_2 fracturing. Shale-acid reactions occur during fracturing or acid stimulation. The mobilisation of metals from these processes can be an environmental concern if production water leaks or is released at surface. In addition, reactions may cause changes at the pore scale and affect gas or fluid flow. Three gas shales from the Australian Cooper Basin REM sequence were characterised for metals in minerals by synchrotron X-ray fluorescence microscopy. Metals including Zn, As, Ni, Cr were hosted in sphalerite associated with organic matter, Pb was in pyrite cement, and Mn was hosted in siderite. The shales were separately reacted with brine and supercritical CO_2, with CO_2-SO_2, with dilute HCl, or with N_2 at 100 °C and 20 MPa in batch reactors. The solution pH decreased during mineral reactions releasing metals to solution with the general concentrations from reaction with HCl > CO_2-SO_2 > CO_2 > N_2 and brine. Of the total available Pb, As, Li, and Zn in the shales, from 0 to 17%, 0.3 to 23%, 3 to 13%, and 0.4 to 28% was released to solution respectively. Corrosion of siderite and ankerite was observed after the CO_2 reactions, with precipitation of Fe-oxides. After CO_2-SO_2 reaction siderite and ankerite were dissolved with pyrite, barite, and Fe-rich precipitates. HCl reactions resulted in complete dissolution of carbonates, with dissolution pits and no mineral precipitation observed. The changes to the fractions of gas accessible mesopores were characterised by small angle neutron scattering (SANS). The Epsilon Formation had the greatest fraction of open accessible pores in the SANS range of 10 to 150 nm, followed by the Murteree and Roseneath shale samples. After CO_2 or CO_2-SO_2 reactions a small decrease in pore accessibility was more pronounced in the Murteree and Roseneath shales, consistent with mineral precipitation. HCl reaction resulted in opening of pores at 150 nm and closing of the smallest measured pores at 10 nm. Metals were mobilised from siderite, ankerite and sulphide minerals mainly, and were dependent on the mineral and metal content but also on the injected gas stream or fluid composition. CO_2 based fluids may result in cleaner flow back water, than HCl based fluids. Geochemical reactions during CO_2 storage or acid treatment in reactive shales cause pore changes that can affect gas migration. Mineral precipitation during CO_2 and CO_2-SO_2 reactions can result in favourable self-sealing.

1. Introduction

The current energy transition, and recent international efforts in extracting hydrocarbons from shale reservoirs have led to increasing interest in shale gas-water interactions (Pearce et al., 2022a; Pearce et al., 2018b; Phan et al., 2018; Renock et al., 2016; Wang et al., 2016;

* Corresponding author at: Centre for Natural Gas, University of Queensland, QLD, Australia.
E-mail address: J.pearce2@uq.edu.au (J.K. Pearce).
[1] Deceased March 18th 2016

https://doi.org/10.1016/j.coal.2023.104271
Received 14 February 2023; Received in revised form 30 April 2023; Accepted 18 May 2023
Available online 20 May 2023

Table 1
Experiment summary, where the brine and the dilute HCl reactions were performed under N_2 pressure. Experiments were performed at 20 MPa and 100ºC in batch reactors.

Shale	Formation	Brine	HCl	CO_2	CO_2SO_2
E1 3266 m	Roseneath	X			X
E1 3491 m	Epsilon		X	X	X
E1 3497 m	Murteree		X	X	X

Table 2
Mineral content (%) of the shale samples from XRD. The content of E1 3491 m after reaction with CO_2SO_2 brine at 100 °C and 20 MPa is also shown. # SEM-EDS indicated that the Mg-siderite contained Ca and Mn signatures and is likely an ankerite. * Indicates minerals identified in trace amounts via SEM. The helium density and total porosity is also shown. Note the mineral components for E1 3266 m and E1 3497 m reported in (Pearce et al., 2018b).

Sample	E1 3266 m	E1 3491 m	E1 3491 m post CO_2SO_2	E1 3497 m
Formation	Roseneath shale	Epsilon Fm	Epsilon Fm	Murteree Shale
quartz	57.1	78.4	68.0	54.5
kaolinite	4.9	5.0	0.2	3.3
illite/muscovite	17.9	10.5	25.4	14.0
siderite	8.3	4.0	1.3	17.0
Mg siderite/ ankerite#	7.5	1.0	0.7	9.0
ankerite (Mn)		0.37		
pyrite	*	0.15		*
chalcopyrite		*		*
sphalerite	*	*	*	*
rutile/anatase	*	*	0.82	*
apatite	*	*	*	*
barite		*	*	
monazite		*		
zircon	*	*	*	*
anhydrite			1.75	
glauconite			1.2	
He density (g/ cm^3)	2.63	2.76		2.81
Porosity (%)	20.5	3.9		21

Table 3
Major elements in the shales reported as % oxides, loss on ignition (LOI) is also shown. Note the compositions for E1 3266 m and E1 3497 m from (Pearce et al., 2018b).

sample	E1 3266 m	E1 3491 m	E1 3497 m
Formation	Roseneath Shale	Epsilon Formation	Murteree Shale
Al2O3	18.2	9.9	10.1
CaO	0.7	0.3	0.2
Fe2O3	8.1	5.3	14.6
K2O	3.2	1.9	1.9
MgO	1.7	1.5	3.1
MnO	0.1	0.1	0.3
Na2O	0.1	0.1	0.1
SiO2	55.1	73.9	55.8
TiO2	0.8	0.7	0.6
H2O	0.6	0.4	0.3
LOI	11.4	5.9	13.0

Wu and Sharma, 2017). Fracture fluid containing chemical such as acids, or CO_2 injected for enhanced recovery or geological storage can react with minerals in shales (Busch et al., 2008; Liu et al., 2016; Tanaka et al., 2016; Tian et al., 2014; Zou et al., 2018). Geochemical mineral dissolution and precipitation reactions in shales can modify properties such as the porosity and permeability, impacting the extraction of oil and gas, or affecting migration of fluids and gases (Ross and Bustin, 2009). Shales can contain high concentrations of metals, and if these metals are present in labile minerals that dissolve they may be released

Table 4
Minor and trace elements (mg/kg) in the shales.

Sample	E1 3266 m	E1 3491 m	E1 3497 m
Formation	Roseneath Shale	Epsilon Formation	Murteree Shale
Ba	692.4	338.2	399.5
Cd	2.8	1.3	4.6
Co	25.0	23.1	28.7
Cr	85.2	40.0	55.0
Cu	138.7	52.5	56.8
Li	70.4	26.4	29.8
Ni	41.8	36.5	45.6
P	1017.6	274.2	729.9
S	425.9	3.5	74.6
Sr	44.2	34.0	33.2
Zn	177.6	57.7	70.9
V	117.8	52.4	63.6
Ga	23.9	16.5	19.8
Ge	6.1	5.5	5.4
As	14.7	16.9	16.4
Se	16.9	5.7	5.6
Rb	195.7	101.2	104.8
Nb	21.5	17.9	15.4
Mo	2.5	1.3	1.4
Sn	35.9	35.8	43.1
Sb	9.2	10.3	5.3
Pb	469.1	26.3	32.0
Th	20.7	13.9	14.5
U	7.6	5.6	5.8

to solution. These reactions, along with oxidation, ion exchange, adsorption and desorption also affect formation water or production water chemistry and water quality by changing pH, electrical conductivity (EC), and concentrations of dissolved major elements and trace metals (Wang et al., 2015). These can include environmentally regulated metals such as Pb, As, Fe, Ba, that may potentially cause environmental issues if large volumes of production water leaks or is accidentally released on the surface. In the USA, for example, 7000–18,000 m^3 of water was estimate to be used in hydraulic fracturing of each unconventional well, with 10 to 80% returned as saline production water, with large volumes of treated wastewater re-injected for disposal (Gregory et al., 2011; Pearce et al., 2022e). Although fracturing has mainly been assessed as likely not significantly contributing to leakage sub-surface, production water leakage has been reported in surface waters downstream of unconventional shale operations (Akob et al., 2016; Osborn et al., 2011). A review of surface water quality in Pennsylvania, USA, reported higher concentrations of Cl and total suspended solids downstream of Marcellus treatment facilities (Olmstead et al., 2013). Studies on potential sources of contamination to shallow aquifers from shale gas activities in the US identified risks from drilling waste disposed of on surface and leached by rainwater, or wastewater leakage from spills, overflow with flooding, or storage pits leaking into groundwater (Bondu et al., 2021; Chapman et al., 2012). In addition fugitive methane leaking into shallow aquifers could release metals and nucleotides (Forde et al., 2019). Poor wastewater treatment may be the main risk, but there is not sufficient data from USA shale gas development, and the need for comprehensive baseline assessments to consider other sources of existing or potential contamination in other countries (Annevelink et al., 2016; Johnson and Graney, 2015).

Several experimental studies have investigated geochemical changes in shale-water or synthetic fracture fluid reactions, mainly focussing on shale formations in the USA such as the Marcellus and Barnett shales (Bratcher et al., 2021; Jew et al., 2017; Zhou et al., 2022b). The reactivity of powdered core and outcrop samples of the Barnett, Marcellus, Green River and Eagle Ford shales with synthetic fracture fluid were compared in batch reactions (Harrison et al., 2017). Dissolution of carbonates and pyrite generated porosity and released metals to solution. However subsequent precipitation of Fe-oxyhydroxides in higher pH conditions was inferred to attenuate the metal contaminant release and occlude pores. Marcon and co-workers reacted Marcellus Shale with

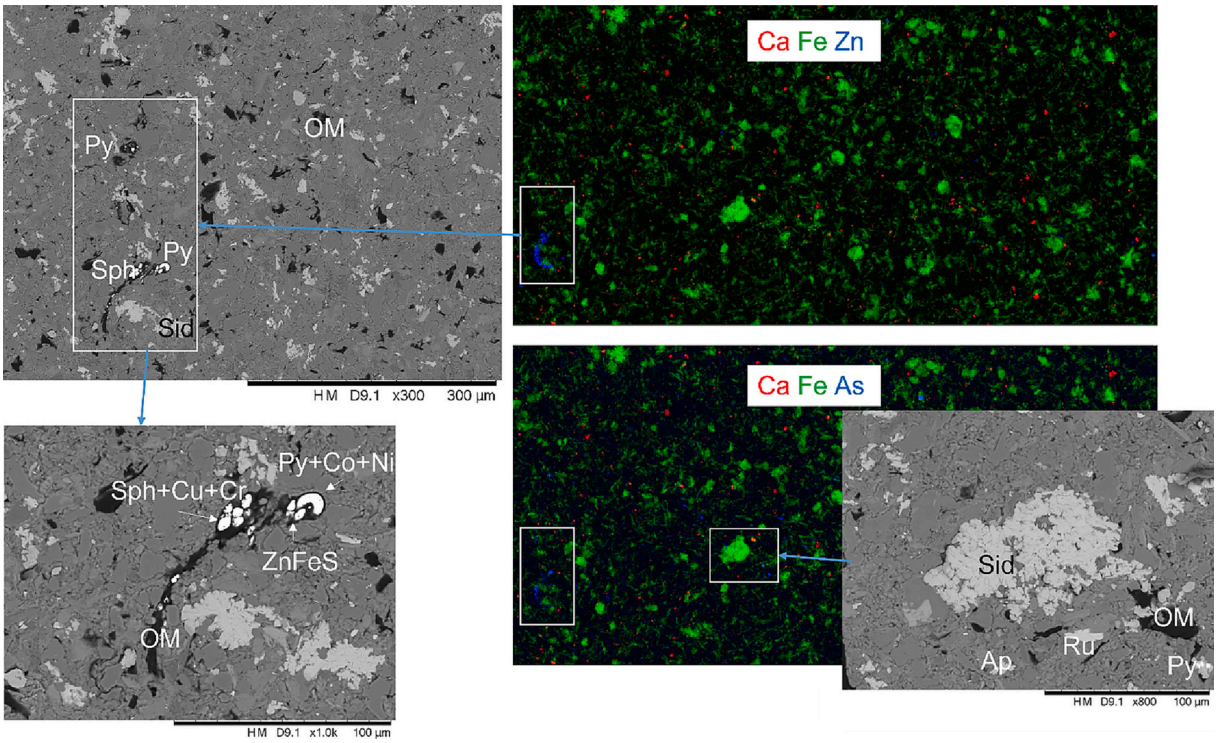

Fig. 1. XFM images for Roseneath Shale E1 3266 m shown as red:green:blue = Ca:Fe:Zn and Ca:Fe:As. Maximum concentrations shown are Ca = 15.5%, Fe = 61.9%, Zn = 6.21%, As = 0.106%. Associated SEM images are also shown corresponding to white boxed areas. Py = pyrite, Sph = sphalerite, Sid = siderite, OM = organic matter, ZnFeS = mixed composition sulphide, Ap = apatite, Ru = rutile. Py + Co + Ni = pyrite with Co and Ni signatures. Sph + Cu + Cr = sphalerite with Cu and Cr signatures. (For interpretation of the references to colour in this figure legend, the reader is referred to the web version of this article.)

simulated fracture fluid in laboratory experiments finding that elements including Co, Cr, Cu, Ni, and Zn were initially released to solution and later decreased, whereas As, Fe, Mn, Sr, and Y remained elevated (Marcon et al., 2017). Carbonate and clay dissolution followed by clay, anhydrite and barite precipitation were observed or predicted. Wilke and co-workers performed leaching experiments on German black shales, finding that the presence of pyrite and calcite controlled pH (Wilke et al., 2015). Metals were released, however they subsequently decreased in concentration through precipitation with overall <15% of the element in the shale mobilised to solution.

The potential for using supercritical CO_2 as a fracturing fluid, or CO_2 enhanced gas recovery (EGR), enhanced oil recovery (EOR) or CO_2 geological storage in shale formations is gaining increasing attention in China and the USA (Liu et al., 2016; Zhang et al., 2021; Zhou et al., 2022a; Zou et al., 2018).

In Australia oil and gas are extracted from conventional sandstone formations, unconventional coal seams (coal seam gas or coal bed methane), and more recently there is increasing activity in gas from shale formations (Barakat et al., 2019; Baublys et al., 2015; Pearce et al., 2021a; Pearce et al., 2022d). There is increasing interest recently in the oil and gas shales of for example the Beetaloo Basin in Northern Australia, or the Eromanga Basin in Queensland and South Australia (Jarrett et al., 2022; Kalinowski et al., 2022; Mao et al., 2023; Troup et al., 2018; Wang and Rezaee, 2020). Both conventional and unconventional oil and gas have been extracted from the Cooper Basin, South Australia. Notably from the Permian shales of the Roseneath-Epsilon-Murteree (REM) sequence in the Nappamerri Trough (Armad, 2014; Hall, 2015; Jadoon et al., 2016a; Jadoon et al., 2016b). Overlying formations such as the Toolachee Formation have also been investigated for CO_2 geological storage near the Moomba processing facility. Recently blue hydrogen storage with CCS has also undergone techno-economic assessment in several reservoirs of the Cooper Basin (Lacey et al., 2022).

Geological storage of CO_2 is gaining increasing interest in the current energy transition to lower emissions to the atmosphere. During CO_2 geological storage CO_2 dissolves in formation water to form carbonic acid during dissolution trapping (Bachu et al., 2005). This can induce dissolution of minerals such as calcite, siderite, feldspars, and chlorite releasing elements to solution and altering porosity and permeability (Ellis et al., 2013; Pearce et al., 2019a; Smith et al., 2013). Subsequently the dissolved CO_2 may combine with dissolved Ca, Fe or Mg to form carbonate minerals or other reactions such as feldspar alteration to kaolinite (Farquhar et al., 2015; Pearce et al., 2021b; Pearce et al., 2022b; Snæbjörnsdóttir et al., 2020). Mineral trapping of CO_2 as carbonate minerals is favourable, however precipitation may plug pores or fines migration can reduce permeability (Pearce et al., 2021c; Pearce et al., 2020; Saeedi et al., 2016). Industrial CO_2 streams from sources such as coal combustion, gas processing, cement, lime, and steel production, can contain a range of types and concentrations of impurity gases including SOx, NOx, H_2S, CH_4, O_2, Ar, and N_2 (Porter et al., 2015; Turner et al., 2022). The separation and capture process itself can introduce impurities such as NH_3, or newer direct air capture may include minor components of N_2 or O_2. Several of these impurity gases can form stronger acids than CO_2 and participate in geochemical rock reactions (Talman, 2015). SO_2 can form sulphuric acid when dissolved in formation water, generating a lower pH than carbonic acid, and reacting with minerals to also form sulphides (e.g. pyrite), sulphates (e.g. anhydrite, gypsum, or barite) or elemental S (Chopping and Kaszuba, 2017; Pearce et al., 2018a; Pearce et al., 2015a). While these precipitated minerals may favourably sequester any mobilised metals, sulphate minerals such as barite may also unfavourably act as scales in the formation, wellbore, or pumps (Cui et al., 2021; Edgin et al., 2021; Marcon and Kaszuba, 2015; Mouzakis et al., 2016; Paukert Vankeuren et al., 2017). An improved understanding of the geochemical reactions occurring during shale-fluid interactions at a range of conditions is needed.

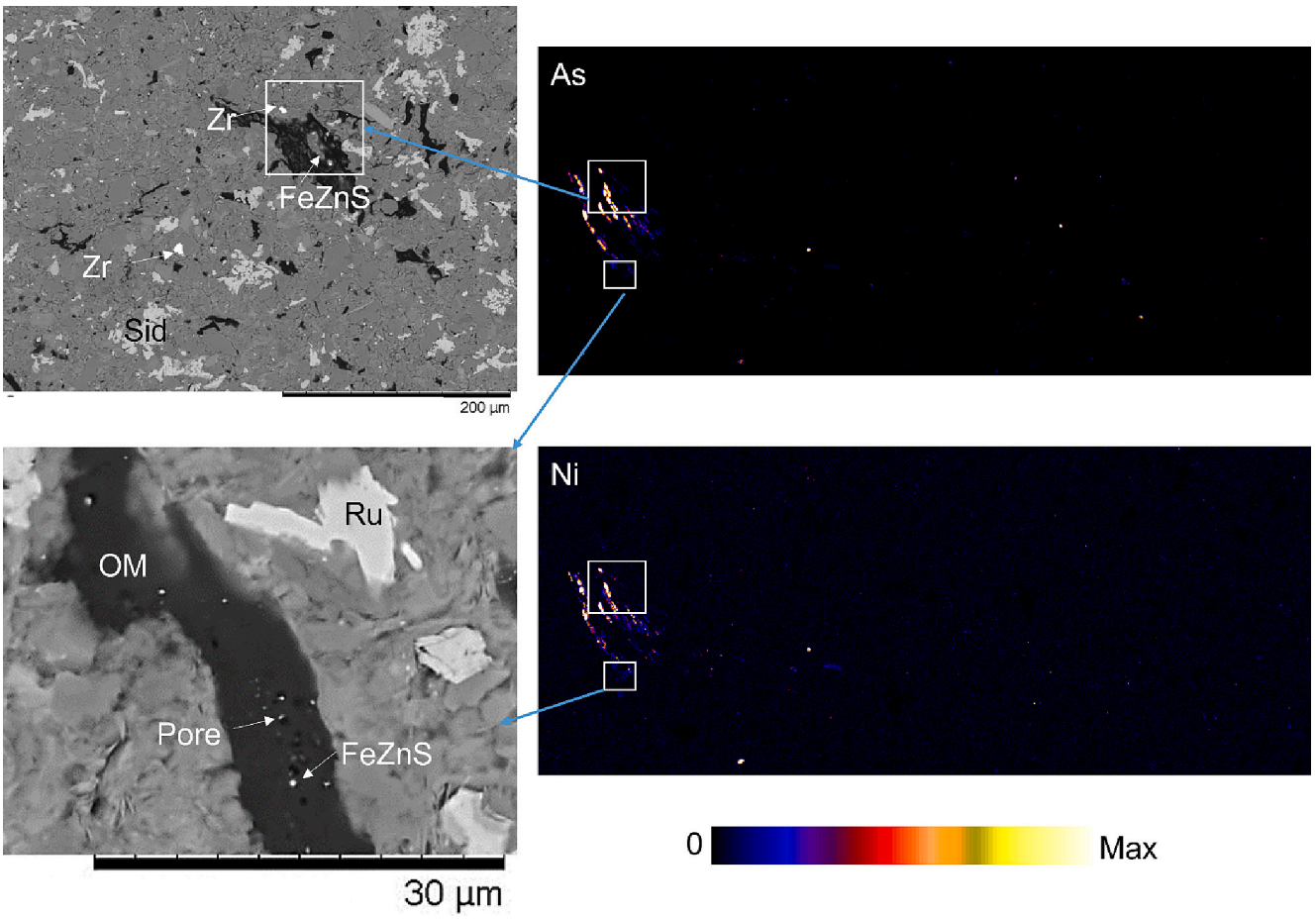

Fig. 2. XFM images of Roseneath Shale E1 3266 m showing concentrations of As (above) and Ni (below), the concentrations legend is shown below. Maximum concentrations shown are As = 0.364% and Ni = 0.824%. SEM BSE images are also shown of white boxed areas. Sid = siderite, Zr = zircon, FeZnS = mixed composition sulphide, OM = organic matter, Ru = rutile. Pores in the organic matter containing sulphides are also labelled.

This study investigates the changes to the fraction of shale accessible *meso* pores and the mobilisation of metals during experimental reactions with brine, dilute HCl, pure CO_2 or CO_2 with an SO_2 impurity under supercritical conditions. The metals hosted in different minerals is assessed via synchrotron X-ray fluorescence microscopy (XFM), with the dissolution and precipitation of minerals investigated for three Australian Cooper Basin shales. The results are applicable to understanding fracturing, enhanced recovery, or CO_2 storage in shale formations.

2. Materials and methods

2.1. Characterisation

Drill core shale samples were collected from the Encounter 1 well core in the REM sequence in the Nappamerri Trough, Cooper Basin, South Australia, described previously (Pearce et al., 2018b). The Cooper Basin shales were selected as gas and oil have been extracted from the Cooper Basin extensively, and shales in this basin are being considered for CO_2 geological storage. The Encounter 1 well core had become open access, and three samples were selected given the limits of the project budget, one from each formation. The three black shales were generally representative of the core. The sample from 3266 m (referred to below as E1 3266 m) is from the Roseneath Shale. The Epsilon Formation sample from 3491 m is hereafter referred to as E1 3491 m. The sample from 3497.27 m is from the Murteree Shale referred to as E1 3497 m.

Core material was powdered and characterised by X-ray diffraction (XRD) with a Bruker D8 Advance diffractometer, the XRD results for two cores were reported previously (Pearce et al., 2018b). Whole rock element characterisation was performed at the University of Queensland (UQ) Environmental Geochemistry Laboratory (EGL). Major elements as % oxides were determined by rock metaborate fusion and analysis by inductively coupled plasma optical emission spectrometry (ICP-OES) (Perkin Elmer Optima 3300 DV ICP-OES instrument, error < 5%), with loss on ignition (LOI). Rock triple acid digestion and analysis by ICP-OES and inductively coupled plasma mass spectrometry (ICP-MS) determined the total minor and trace elements (Thermo Electron X-7 Series quadrupole ICP-MS, error 5–10%). Mercury injection capillary pressure porosimetry (MICP) was performed to determine pore throat size distributions with a Micromeritics AutoPore IV 9500. Helium pycnometry was also performed with a Micrometrics AccuPyc II 1340. Cumulative and differential CO_2 pore volume was measured on a Micrometrics TriStar II 3020 for one sample before and after reaction.

Scanning electron microscopy with energy dispersive spectroscopy (SEM-EDS) was performed on core surfaces before and after reactions with either a JEOL 6460LA environmental SEM or Hitachi TM3030 with a Brucker EDS detector. This was also performed on polished thin sections after X-ray Fluorescence Microscopy (XFM) to confirm the mineral phases present in the scanned areas.

Polished 30 µm thin sections were prepared on fused quartz slides for XFM at the XFM beamline of the Australian Synchrotron (Ryan et al., 2014). Slides were fixed to a Perspex plate sample holder with Mylar tape in the instrument translation stage. On-the-fly scanning fluorescence microscopy was performed with the Maia detector, and Kirkpatrick-Baez mirrors focussing the X-ray beam (18.5 KeV) to ~2 µm. Scans were run at up to 2 µm spatial resolution and 10 msec/pixel dwell-time (Howard et al., 2020; Paterson et al., 2011; Pearce et al., 2021a;

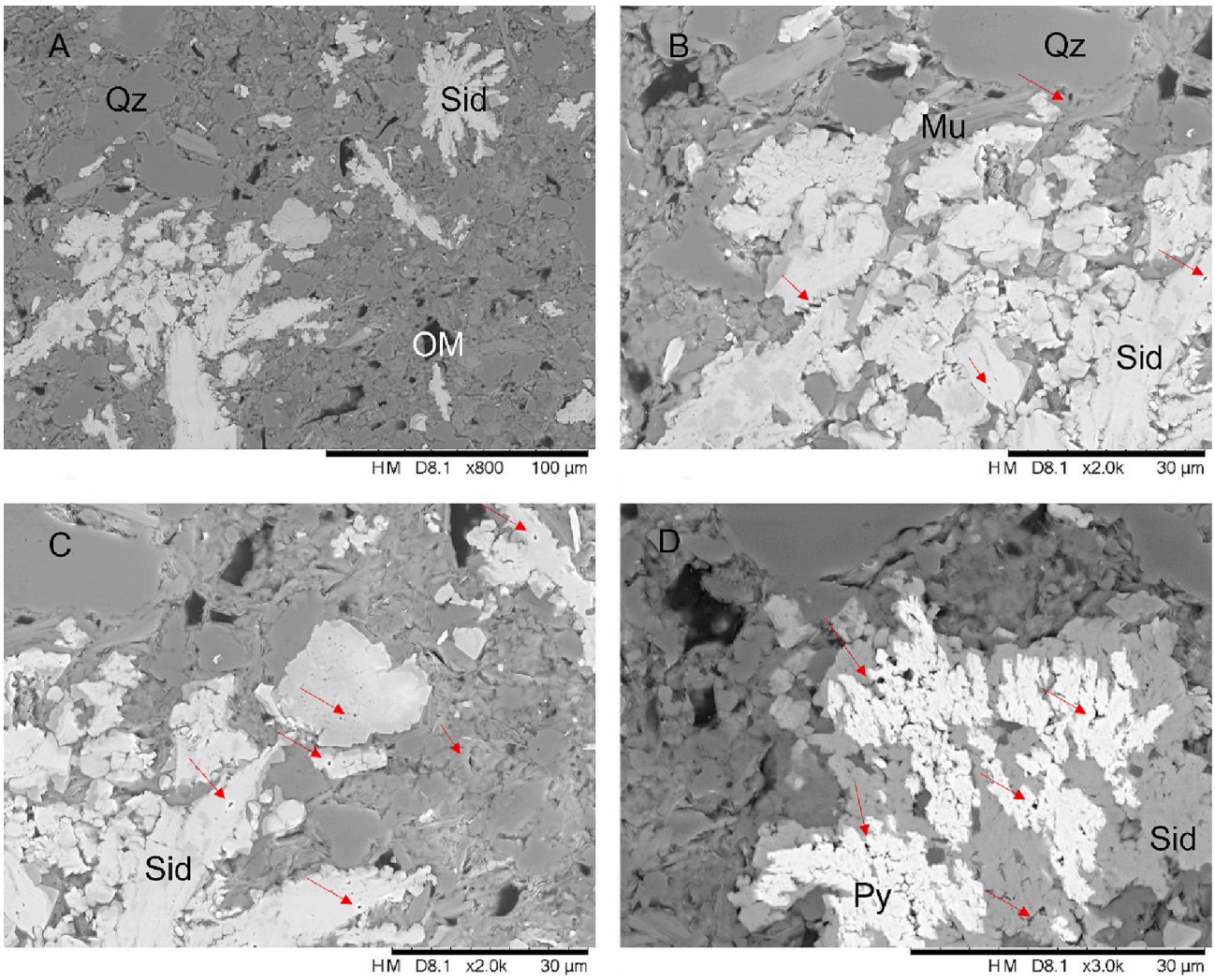

Fig. 3. SEM BSE images of Roseneath Shale E1 3266 m. A) Unusual morphology siderite cements, quartz grains and organic matter in the clay matrix. B) Pores marked by red arrows in siderite. C) Pores in siderite and clay matrix marked by red arrows. D) Pores in pyrite cements surrounded by siderite. Py = pyrite, Qz = quartz, Sid = siderite, OM = organic matter, Mu = muscovite. (For interpretation of the references to colour in this figure legend, the reader is referred to the web version of this article.)

Pearce et al., 2022b; Pearce et al., 2022c; Ryan et al., 2010). Standards were run daily, with images generated with GeoPIXIE (Ryan et al., 2014).

The Small Angle Neutron Scattering (SANS) method has been described previously for different samples run concurrently (Pearce et al., 2018a). Shales and selected reacted samples were hand polished perpendicular to bedding plane to 15 mm diameter discs of 1 mm thickness. A custom-built high temperature and pressure cell was used at the general-purpose SANS beamline (GP SANS), Oak Ridge National Laboratory (ORNL), High Flux Isotope Reactor (Wignall et al., 2012). A Q range of 0.003–0.76 $Å^{-1}$, with neutron wavelengths 4.72 Å and 6 Å and a $\Delta\lambda/\lambda$ resolution 0.13 were used. Samples were run at both ambient conditions and with pressurized deuterated methane (6500–7500 psi) contrast matching fluid for zero average contract (ZAC) conditions. Both 18.5 m and 0.3 m sample to source distances were run (Bahadur et al., 2015; Melnichenko et al., 2012; Ruppert et al., 2013). At the contrast matching ZAC condition, the scattering length density of accessible pores filled with pressurized methane are equal to the rock scattering power so net scattering is only from inaccessible pores. Data were corrected and calibrated with standards and scattering vector to pore radius relation $r \approx 2.5/Q$ was used to relate the data to pore radii as the fraction of gas accessible pores (ϕ AC).

2.2. Reaction experiments

Reaction experiments were performed in a PEEK lined high pressure and temperature reaction rig based on Parr reaction vessels that has been described in detail previously (Pearce et al., 2015a; Pearce et al., 2015b). Shales solid blocks and discs were generally separately submersed in 100 ml of deoxygenated low salinity brine (NaCl 585 mg/l) at a water:rock ratio of 10 at 100 °C. The reaction conditions were limited by the reaction rig available that was run at the maximum operating temperature of 100 °C, and a reasonable in situ subsurface pressure of 20 MPa. Experiments were run at water:rock ratios of 10 to enable enough fluid for sampling and analysis of the fluid after reaction. Note that this water:rock ratio is likely to be higher than subsurface conditions.

The reactors were flushed with N_2 to remove residual air. A subsample of E1 3266 m was pressurized with 20 MPa N_2 with a Teledyne injection pump. A second sub sample of E1 3266 m was pressurized with 20 MPa supercritical CO_2 containing 0.2% SO_2. Experiments were run for 3 days and are summarized in Table 1, all reactions were unstirred batch type reactions. Experiments were generally run for three days consistent with an acid or fracture stimulation and shut in. The E1 3491 m and E1 3497 m shales were pressurized with 20 MPa pure supercritical CO_2, or separately with supercritical CO_2 with 0.2% SO_2 for 3

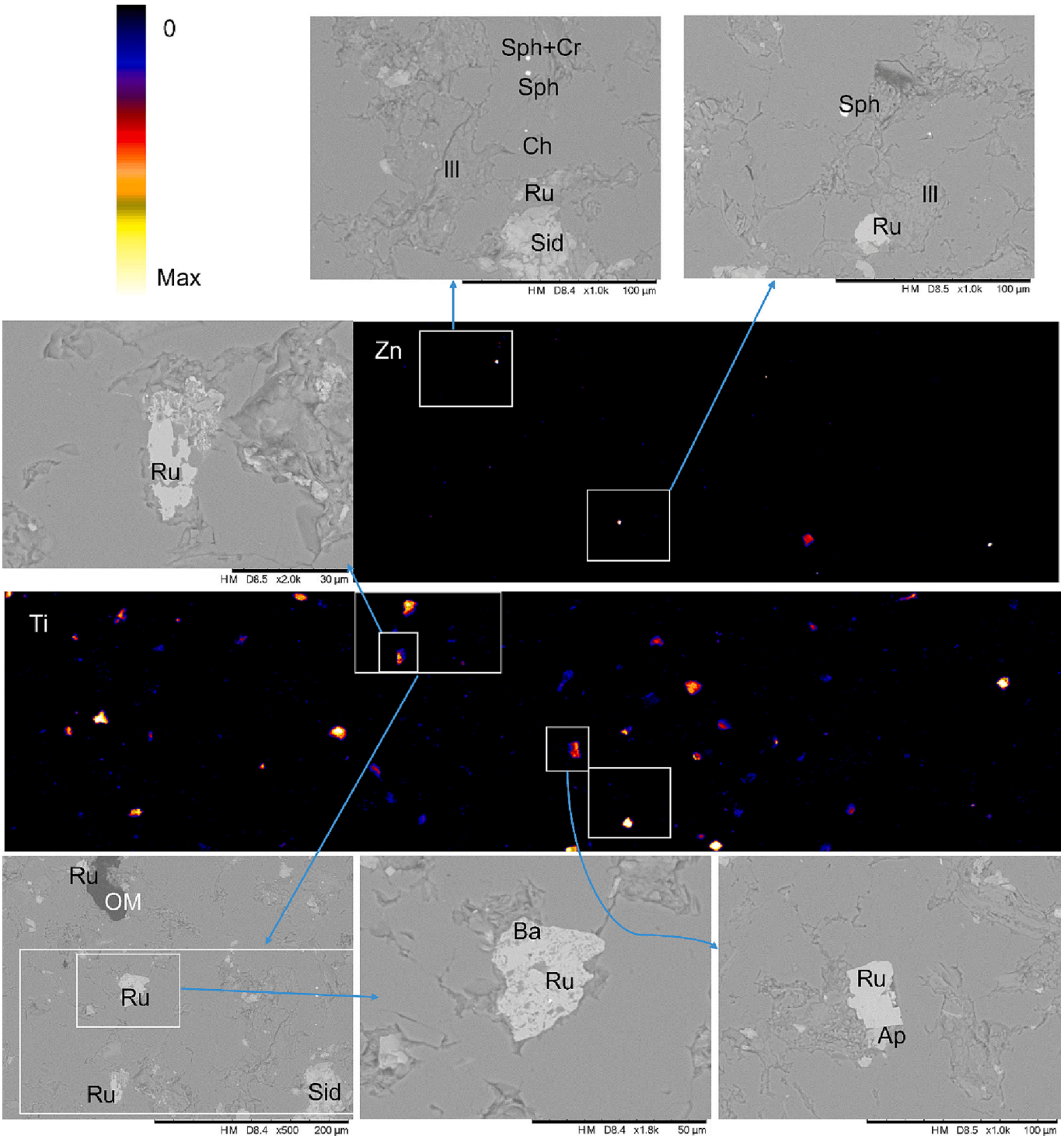

Fig. 4. XFM images of Zn and Ti concentrations for Epsilon Formation E1 3491 m, the legend is also shown in the top left where black = 0 to yellow = maximum. The maximum concentrations shown are Ti = 55%, Zn = 5.41%. Corresponding SEM images of white boxed areas are also shown. Ch = chalcopyrite, Sph = sphalerite, Sid = siderite, OM = organic matter, Ill = illite, Ap = apatite, Ru = rutile, Ba = barite. Sph + Cr = sphalerite with Cr signatures. (For interpretation of the references to colour in this figure legend, the reader is referred to the web version of this article.)

days. In addition, E1 3491 m and E1 3497 m were also separately reacted in dilute HCl (1%) pressurized to 20 MPa N_2. At the end of reactions, the pH and conductivity were measured immediately with a TPS meter and probes (TPS WP81, error ± 0.01), and fluid was sampled for analysis of cations and anions. Blank experiments with no rock sample present were also run at the same conditions to check for any metals released from the reactor (supplementary material).

Fluid subsamples were filtered (0.45 µm), diluted 10×, acidified with 2% ultra-pure nitric acid and analysed by ICP-OES for major and minor ions, and ICP-MS for minor and trace ions at the University of Queensland Environmental Geochemistry Laboratory. Subsamples (not acidified) were also analysed for dissolved SO_4 concentration at ALS Environmental, Brisbane.

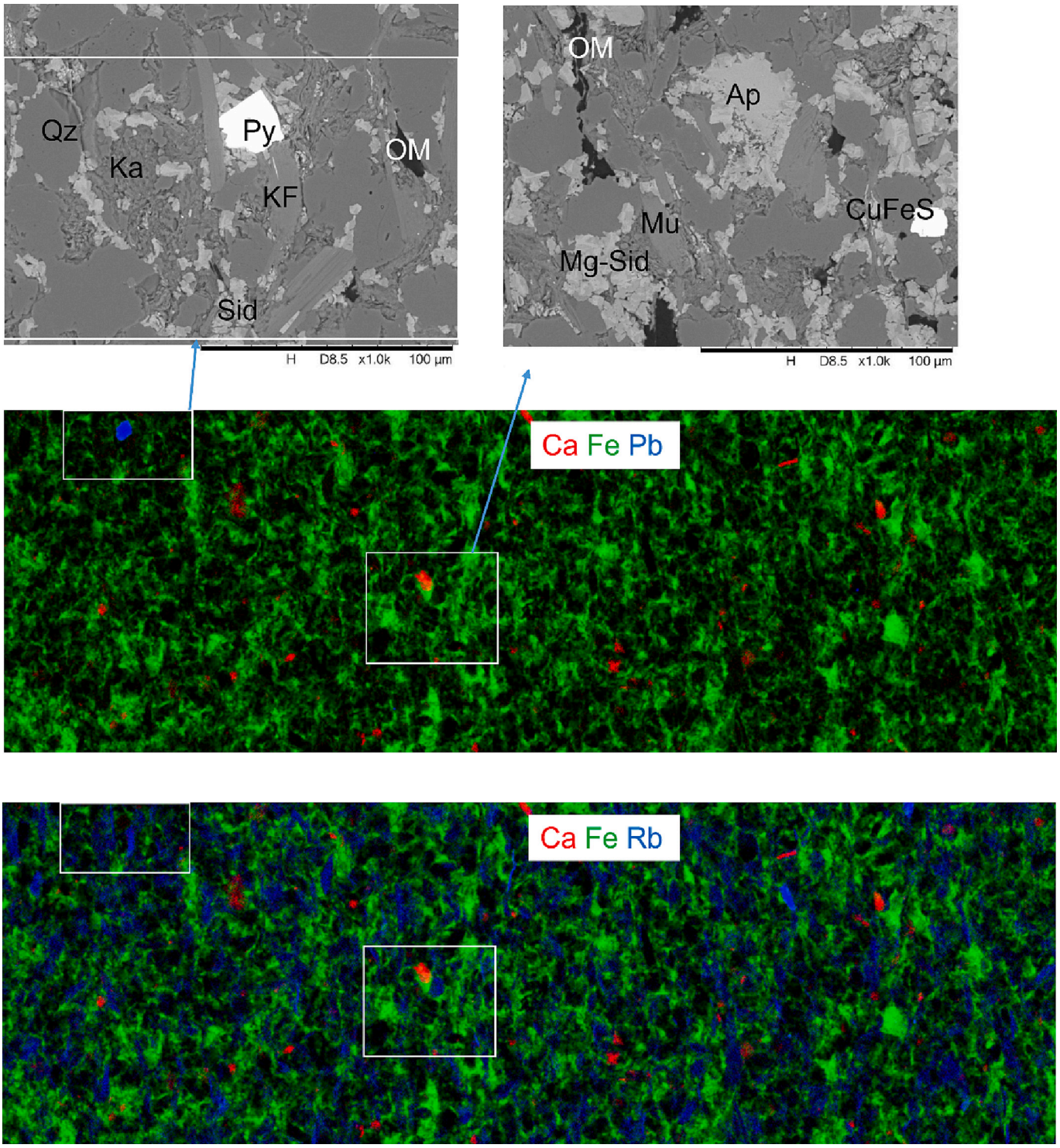

Fig. 5. XFM images of Murteree Shale E1 3497 m shown as red:green:blue = Ca:Fe:Pb and Ca:Fe:Rb. Maximum concentrations shown are Ca = 42.3%, Fe = 57.3%, Pb = 16.6%, Rb = 0.103%. SEM BSE images of the corresponding white box regions are also shown. Qz = quartz, Py = pyrite, Ka = kaolinite, KF = K-feldspar, Sid = siderite, OM = organic matter, CuFeS = mixed composition sulphide, Ap = apatite, Mu = muscovite, Mg-Sid = Mg-siderite/ankerite. (For interpretation of the references to colour in this figure legend, the reader is referred to the web version of this article.)

3. Results and discussion

3.1. Characterisation

The three core samples are black shales, the Epsilon Formation E1 3491 m contained a higher proportion of quartz. All contained kaolinite, illite/muscovite, and siderite/ankerite with trace amounts of other minerals including sulphides, apatite, barite, monazite, and zircon (Table 2). The total major and minor element content of the shales are shown in Table 3 and Table 4. Roseneath shale E1 3266 m generally contained a higher concentration of S, Cr, Cu, Pb, Zn, V and Ba (Table 4) that may be associated with visually more pyrite and sphalerite cements observed in SEM that are associated with siderite and organic matter (Figs. 1-3).

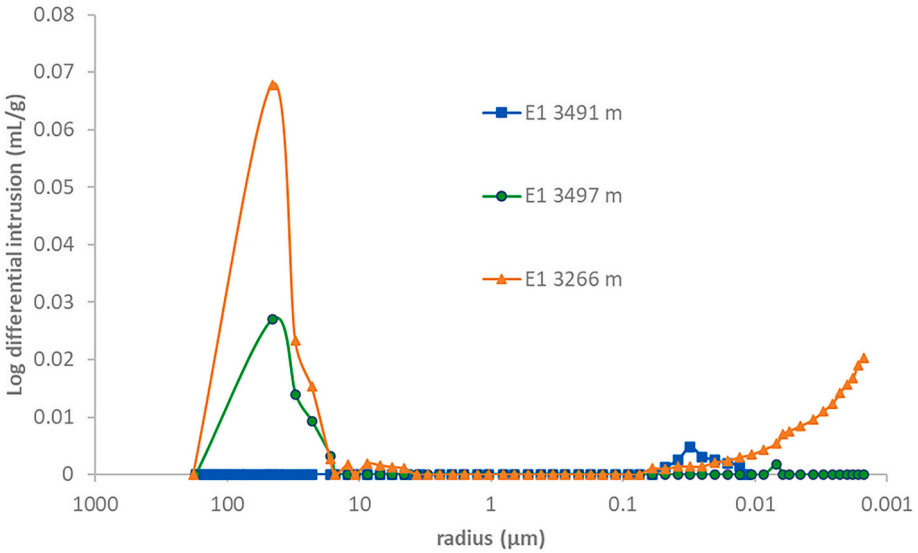

Fig. 6. MICP pore throat diameter distributions. E1 3266 m is Roseneath Shale (orange), E1 3491 m is Epsilon Formation (blue), E1 3497 m is Murteree Shale (green). (For interpretation of the references to colour in this figure legend, the reader is referred to the web version of this article.)

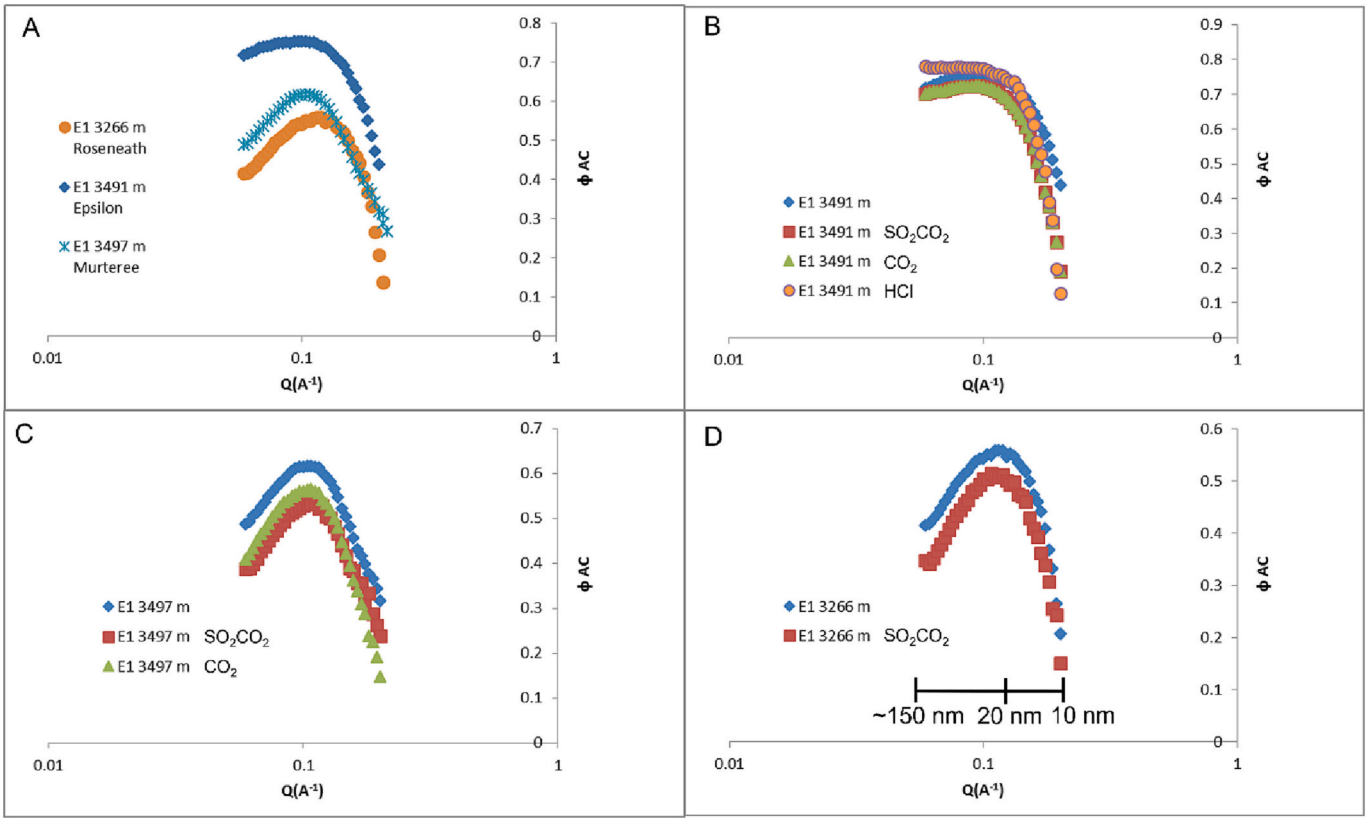

Fig. 7. Fractions of SANS accessible porosity. A) The three unreacted shale samples. The data from left to right correspond to pore radii of ~150 nm to ~10 nm. B) Epsilon Formation E1 3491 m before and after reactions. C) Murteree Shale E1 3497 m before and after reactions. D) Roseneath Shale E1 3266 m before and after reactions. The corresponding approximate pore size is shown in D. All reactions were at 20 MPa and 100 °C in unstirred batch reactors.

Total organic carbon (TOC) has been reported for samples of the Roseneath Shale, Epsilon Formation, and Murteree Shale in this well (Encounter 1) at 3, 6.7, and 2.2% respectively. Previous measurements for the Murteree Shale and Epsilon Formation in the Cooper Basin were 1.7 to 4.7% (average 3%) and 0.1 to 9.8% (average 4%) respectively. The Roseneath and Murteree shales are reported as type III (III/IV) kerogen dry gas prone, and the Epsilon Formation type II kerogen oil prone (II/IV to II). Nanopores were also reported in organic matter and clays in the three formations (e.g. Murteree ~25 to 250 nm) in the well completion report and other studies (Jadoon et al., 2016a; Jadoon et al., 2016b).

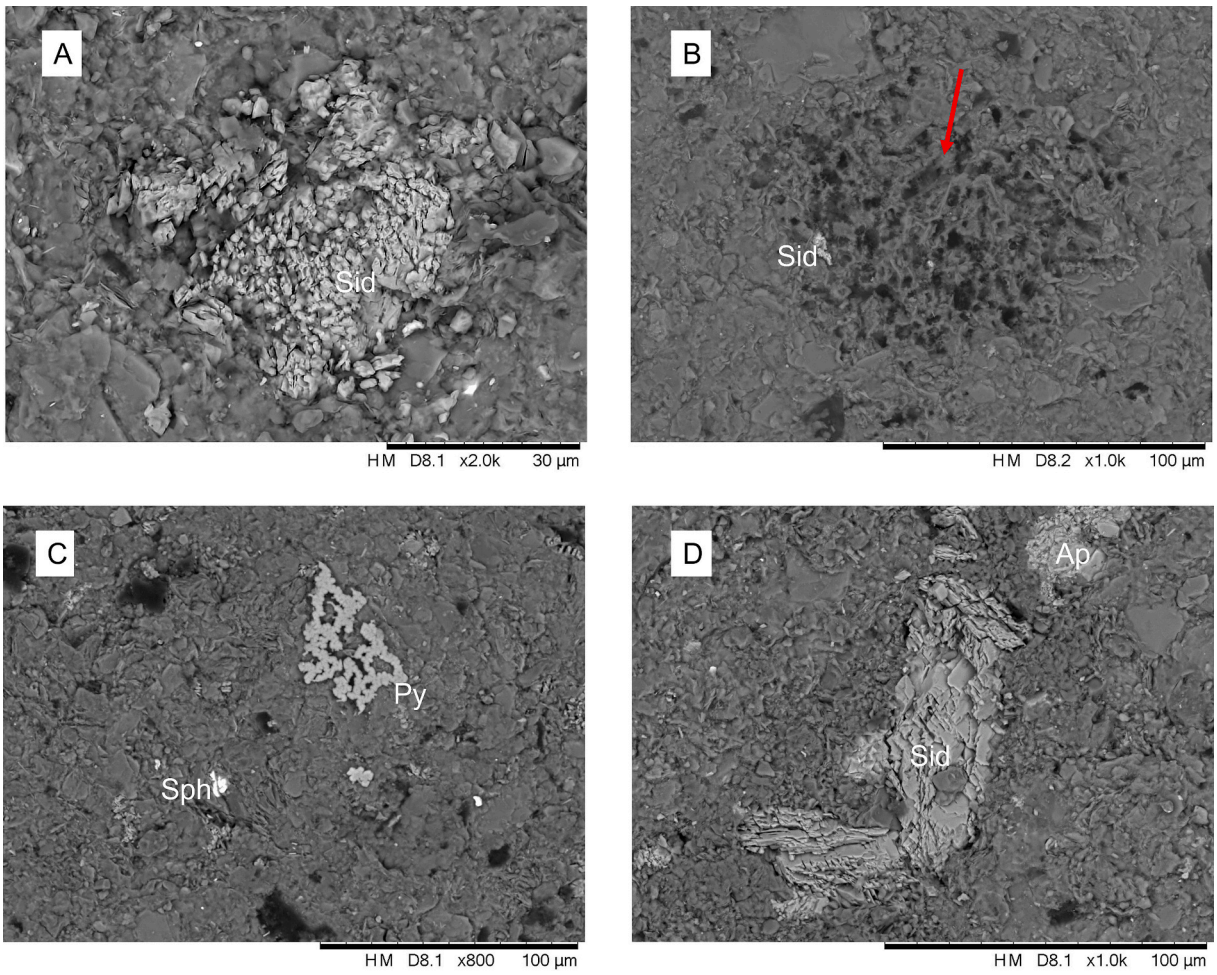

Fig. 8. SEM BSE images of Roseneath Shale E1 3266 m after CO_2SO_2 and brine reaction at 100 °C and 20 MPa. A) Corroded siderite. B) Dissolution pitting (red arrow) and residual siderite. C) Sphalerite, and precipitated pyrite cements. D) Etched siderite cements. Sid = siderite, Sph = sphalerite, Py = pyrite, Ap = apatite. (For interpretation of the references to colour in this figure legend, the reader is referred to the web version of this article.)

3.2. Synchrotron XFM

The Roseneath shale E1 3266 hosted As, Ni, Cu, Cr, and Zn in sphalerite associated with organic matter (Fig. 1, Fig. 2, and supplementary material). Mn was mainly hosted in siderite (supplementary material). Pb was mainly present in both sphalerite and pyrite in organic matter and was also occasionally in siderite. Pyrite was also observed that contained Co and Ni and was in organic matter.

The Epsilon Formation sample E1 3491 hosted Zn and Cr in sphalerite (Fig. 4), however this was in the rock matrix not in organic matter (unlike sphalerite in E1 3266). In addition, As *was not* associated with sphalerite in this case and was often co-located with Ni, although the host was not identified. Pb was in siderite and pyrite, and also occasionally in K-feldspar (supplementary material). Sr was in K-feldspar, and Rb hosted in illite. Monazite hosted U and Ni. Rutile (Ti), Barite cements (Ba), and apatite (Ca) were also present.

In the Murteree Shale, E1 3497 m, Ca was again mainly hosted in apatite with Pb hosted in pyrite cement (Fig. 5). Rb was in muscovite/illite and K-feldspar (Fig. 5). Cu was hosted in chalcopyrite and mixed sulphides in the rock matrix (supplementary material). Both As and Ni tended to be co-located and appeared to be associated with organic matter (supplementary material).

3.3. Pore character and changes after reactions

The total accessible porosity of the three shales was determined by mercury injection capillary porosimetry (MICP) and helium pycnometry (Table 2). The Epsilon Formation, E1 3491 m, sample had the lowest total porosity of the three shales, but the MICP showed pore volume (within the MICP measurement range) was mainly in pores at ~15 to 100 nm (0.015 to 0.1 µm) (Fig. 6).

The accessible pore fraction between ~10 to 150 nm was measured by SANS. The Epsilon Formation has the highest accessible porosity fraction of the three shales in the size range of SANS (Fig. 7a, and supplementary material), that was also consistent with the MICP pore volume. The Roseneath and Murteree shale samples had the majority of accessible pores in the size range ~ 40 to 50 nm in SANS. The Roseneath Shale had the lowest accessible pore fraction in SANS of the three shales, especially at the smallest measured size ~10 nm (Fig. 7a). The reason for the higher accessible *meso*porosity of the Epsilon Formation is not clear. The Roseneath and Murteree shales are reported as dry gas prone source rocks (type II to IV), however the Epsilon Formation is type II to III oil/gas (BeachEnergy, 2011; GA, 2017; Granger, 2013). Solid bitumen in the Epsilon may be hosting more organic porosity (İnan et al., 2018).

The Epsilon Formation E1 3491 m, at ~150 nm pore size had a SANS accessible porosity fraction of 0.71 that increased to 0.78 after HCl reaction. The accessible porosity fraction at ~150 nm however remained the same at 0.71 after both CO_2 or CO_2SO_2 reaction (Fig. 7b). At ~10 nm the accessible porosity fraction decreased from 0.44 to 0.13 after HCl reaction. The accessible pore fraction at 10 nm also decreased to 0.2 after CO_2 or CO_2SO_2 reaction.

The CO_2 adsorption was separately measured on E1 3491 m in the

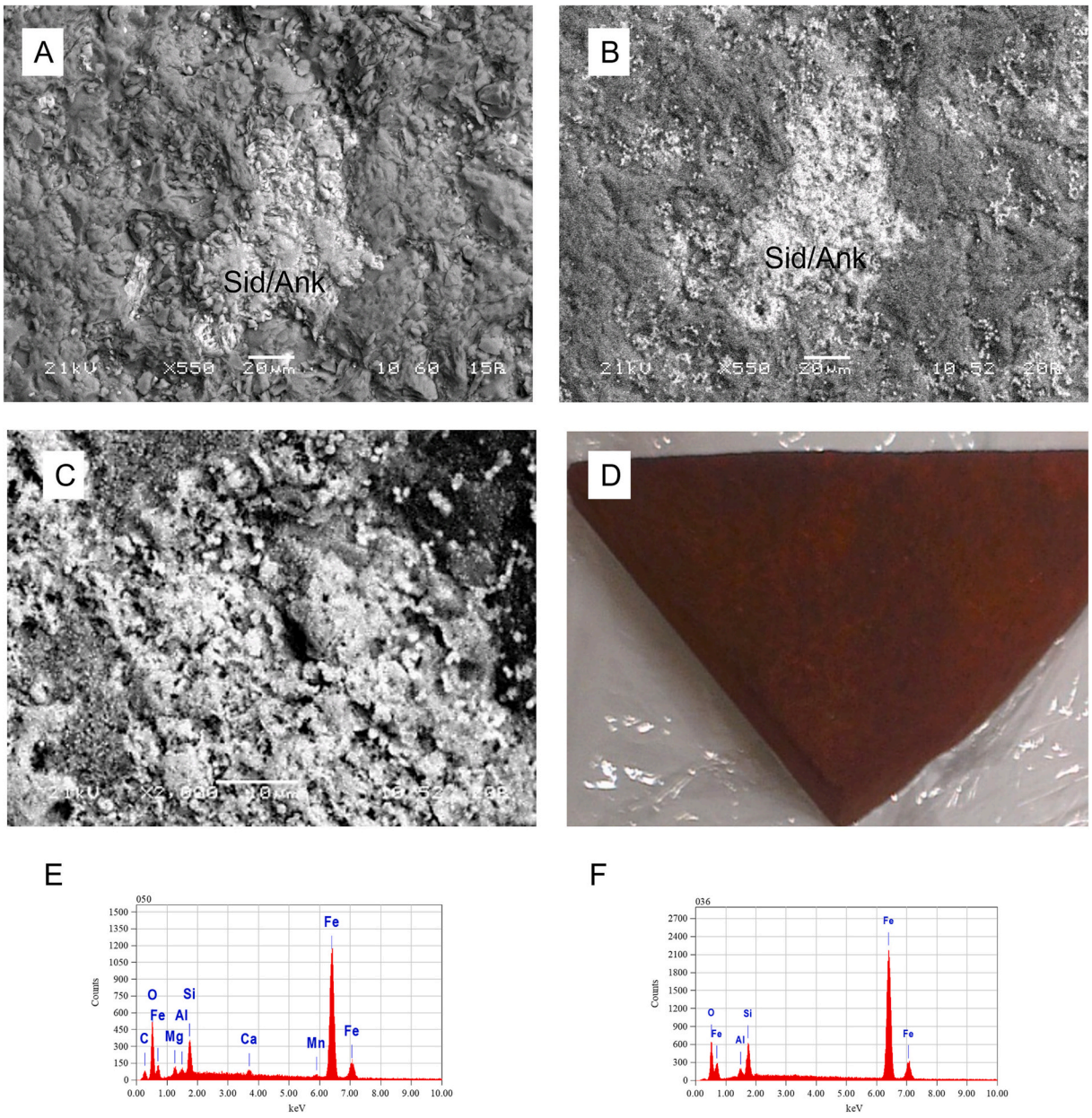

Fig. 9. SEM BSE images of Epsilon Formation E1 3491 m. A) Siderite/ankerite before reaction. B) The same region in A after supercritical CO_2 and brine reaction at 100 °C and 20 MPa. Showing siderite/ankerite corrosion and fine iron rich precipitates. C) Fine precipitates after the CO_2 reaction. D) Photo showing the red brown precipitates on the shale surface after the CO_2 reaction. E) EDS of siderite/ankerite before reaction. F) EDS of Fe-rich precipitates after the CO_2 reaction. (For interpretation of the references to colour in this figure legend, the reader is referred to the web version of this article.)

0.8 to 0.4 nm pore size range before and after the CO_2SO_2 reaction. The pore volume decreased after CO_2SO_2 reaction (supplementary material).

Accessible porosity fractions generally decreased in the Roseneath Shale E1 3266 m after CO_2SO_2 reaction (Fig. 7c and supplementary material). For larger pores ~150 nm the accessible porosity fraction decreased from 0.42 to 0.35 after reaction. The smallest measured pores ~10 nm also had a decrease in accessible porosity from 0.21 to 0.15. Accessible porosity fractions decreased in the Murteree Shale E1 3497 m after CO_2 or CO_2SO_2 reactions (Fig. 7d). Accessible pore fractions in the Murteree at ~150 nm decreased from 0.49 to 0.41 after CO_2 reaction, and to 0.39 after CO_2SO_2 reaction. At ~10 nm accessible porosity decreased from 0.32 before reaction to 0.15 after CO_2, and 0.24 after CO_2SO_2 reaction.

The shale reactions with dilute HCl at 100 °C and 20 MPa N_2 resulted in the dissolution of siderite/ankerite that revealed underlying illite pores. An increase in gas accessible *meso* pores ~150 nm was measured in SANS after the HCl shale reaction, consistent with the revealing of clay porosity, however the smallest measured meso pores closed. The pure CO_2 and CO_2-SO_2 reactions of shales in brine at 100 °C and 20 MPa resulted in partial dissolution of carbonates, however precipitated minerals also coated surfaces likely blocking pores. The SANS methane accessible meso pores decreased after CO_2 and CO_2-SO_2 reactions of the shales. This is consistent with precipitated mineral coatings closing gas accessible meso pores. This is also consistent with a study on shale caprock where SANS gas accessible porosity also decreased on impure CO_2 (SO_2, O_2) reaction (Pearce et al., 2018a). Micron sized pores in siderite and illite, and at the organic matter-clay interface have been reported previously in these shales (in the Encounter 1 well completion report) (BeachEnergy, 2011). Illite has also been reported to contain pores ~20 nm, with organic matter nanopores observed in the range ~

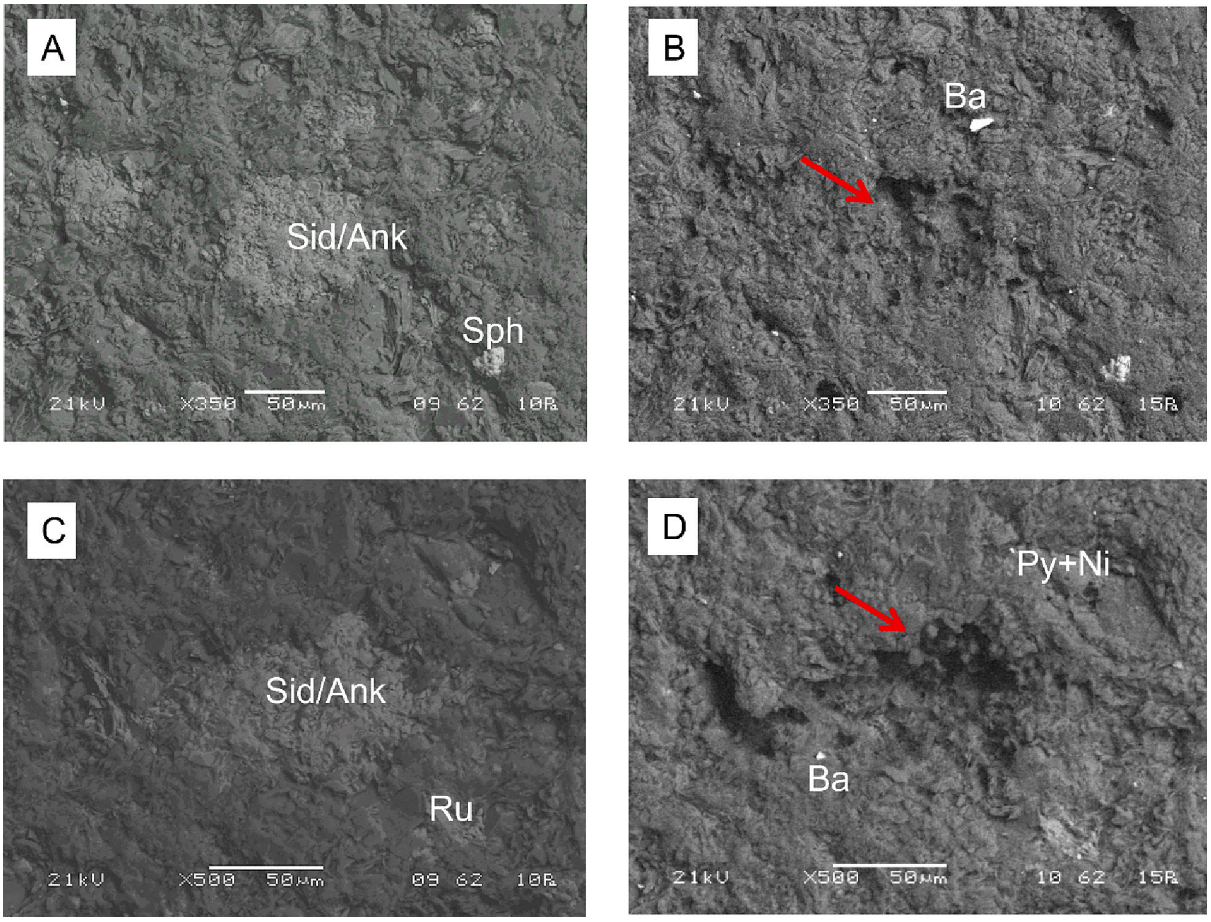

Fig. 10. SEM BSE images of Epsilon Formation E1 3491 m. A) Siderite and ankerite cements and sphalerite before reaction. B) Same region in A after CO_2SO_2 and brine reaction at 100 °C and 20 MPa, with siderite/ankerite dissolved leaving a surface pit (red arrow), and barite precipitate. C) Siderite/ankerite and rutile before reaction. D) Same region in C after the CO_2SO_2 reaction, siderite has dissolved leaving a surface pit (red arrow), and fine barite and pyrite+Ni precipitates. Sid/Ank = siderite/ ankerite, Sph = sphalerite, Ba = barite, Ru = rutile Py + Ni = pyrite with Ni signtures. Sid/Ank had a FeMgCaMn signature in EDS of a Ca containing siderite or siderite/ankerite mixture. (For interpretation of the references to colour in this figure legend, the reader is referred to the web version of this article.)

25–300 nm in other samples of these shales (BeachEnergy, 2011). Other Australian shale from the Beetaloo Subbasin, NT, has also been reported to host gas mainly in illite pores where it is organic matter poor (Sander et al., 2018). The Marcellus Shale in the USA hosts porosity in both organic matter and clays (Bahadur et al., 2018). Canadian Jurassic shales were also reported to host CH_4 or CO_2 in both organic matter and in illite and montmorillonite pores (Ross and Bustin, 2009). Niutitang Shale samples from China were reported to host the majority of pores in organic matter but also in illite (Sun et al., 2018). The pore volume measured in the current study by CO_2 adsorption of the Epsilon Formation sample after CO_2-SO_2 reaction decreased in the size range 0.8 to 0.4 nm in general in agreement with the decrease in SANS gas accessible porosity. The overall decrease in the smaller pore gas accessibility ~10 nm and < 1 nm in reactions may be associated with changes to organic matter such as swelling or precipitation of coatings in the smaller organic matter pores. Very recently a calcite rich shale from Morocco was shown via synchrotron in situ micro CT imaging to undergo organic matter and clay swelling from water, reducing porosity by 50% (Wang et al., 2023). It is possible the low salinity brine in the current experiments is also causing organic matter swelling closing the smallest shale pores, however further work out of the scope of this study would be needed to confirm the different mechanisms occurring.

3.4. SEM-EDS before and after reactions

After the supercritical CO_2 reactions with brine at 20 MPa pressure and 100 °C, all shales had a precipitated layer with a red-brown colouration to the eye, and after CO_2 SO_2 reaction a dark yellow-brown colouration.

After reaction with brine under 20 MPa pressurized N_2 at 100 °C, the Roseneath shale, E1 3266 m, had a more roughened surface in SEM, with precipitated Fe-oxides, barite, and a Cr—Ni containing precipitate likely an oxide (supplementary material Fig. S13). In the CO_2 SO_2 brine reaction of the Roseneath shale, siderite was corroded or in places completely dissolved leaving pits in the surface (Fig. 8, and supplementary material Fig. S14), with precipitated pyrite cements.

After supercritical CO_2 reaction of the Murteree shale in brine, E1 3497 m, siderite/ankerite was corroded, with precipitation of fine-grained Fe-oxides (supplementary material Fig. S15). The Epsilon Formation, E1 3491 m, was also reacted with supercritical CO_2, with siderite/ ankerite corrosion observed after reaction, and fine-grained Fe-oxides precipitated mainly on the siderite surfaces (Fig. 9, and supplementary material Fig. S16). In the CO_2 SO_2 brine reaction of Epsilon Formation E1 3491m, siderite/ankerite was generally completely corroded, with precipitation of barite and fine-grained pyrite containing Ni (Fig. 10). In the dilute HCl reaction of E1 3491 m under N_2, total dissolution of carbonate cements left pits in the surfaces revealing underlying clays (Fig. 11). No precipitates were observed on rock surfaces via SEM after the shale dilute HCl reactions.

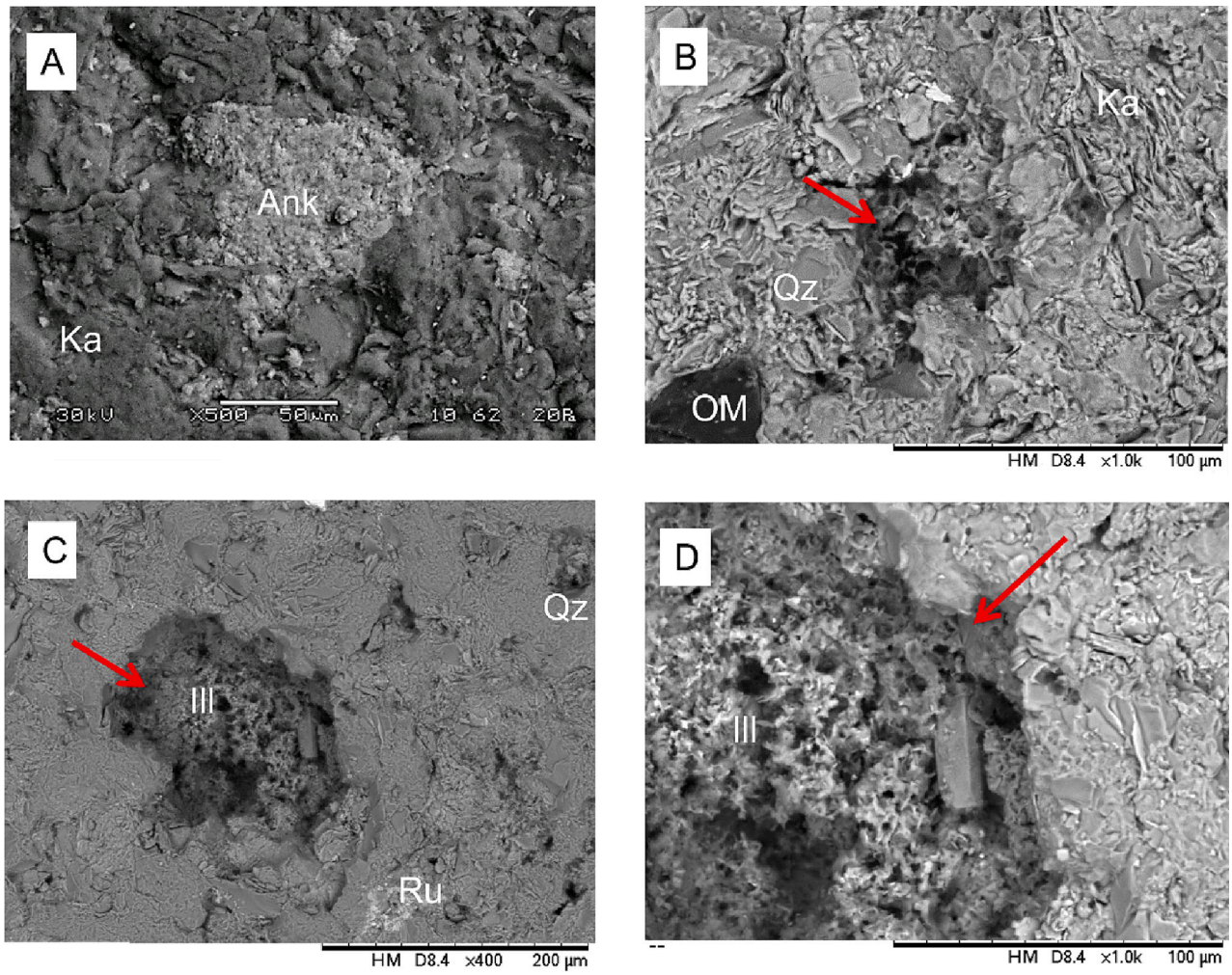

Fig. 11. SEM BSE images of Epsilon Formation E1 3491 m. A) Ankerite before reaction. B) Corrosion pits (red arrow) after dilute HCl reaction at 100 °C and 20 MPa. C) Corrosion pit after the HCl reaction, with roughened rock surfaces. D) Pore filling illite revealed in the dissolution pit after the HCl reaction. Ank = ankerite, Ka = kaolinite, Qz = quartz, OM = organic matter, Ill = illite, Ru = rutile. (For interpretation of the references to colour in this figure legend, the reader is referred to the web version of this article.)

3.5. Water chemistry and reaction metal release

The generated solution pH was lowest at the end of the dilute HCl reactions (pH 1 to 1.1), and highest after the pure CO_2 (pH 5.2 to 6) or brine (pH 5.4) reactions (supplementary material). The Roseneath Shale CO_2 SO_2 reaction also had a low pH of 1.2 likely owing to additional sulphide mineral reaction releasing dissolved S generating sulphuric acid and lowering solution pH (the pH, EC and sulphate concentrations are given in supplementary material).

Dissolved major, minor and trace elements released to solution in the experiments are shown in Figs. 12 – 14 and in the supplementary material. In general the highest element concentrations were released in the dilute HCl reactions. The element release to solution as a percentage of the total element content in the shale rock sample is shown in Table 5. Relatively high percentages of elements As, Pb, Ba, Li, and Zn were released to solution from the Epsilon Shale E1 3491 m reaction with HCl.

In the CO_2SO_2 and brine blank experiment with no shale present 16 mg/l of Fe and 1 mg/l of Cr were released from the reactor (supplementary material). The dilute HCl blank experiment released 3.7 and 0.7 mg/l of Fe and Cr respectively. These represent a possible background of ~6 to 15% of the total dissolved concentrations released in the shale reactions, however it is likely that lower background concentrations were released during shale reactions as the pH was buffered in the presence of the rock.

Metal content and metal release to solution on reaction was dependant on the metal content of the shales but also the reaction fluids, the generated pH and the mineral content. Overall, the shales released metals to solution with the concentrations released greatest in the HCl reactions with the lowest pH: HCl > CO_2-SO_2 > CO_2 > N_2 and brine. Environmentally sensitive elments such as As, Pb, Ba and Zn than can be a risk to health were released as the highest proportion of the rock content from the Epsilon Formation E 3491 m reaction with HCl at 21, 17, 10 and 28% of the total available respectively. This is in reasonable agreement with Wilke and co-workers who reported <15% of total metals available in German black shales were mobilised by long term simulated fracture fluid reactions at 100 °C (Wilke et al., 2015). They found that the released metals were dependent on the mineral content of the shale and especially the buffering capacity controlled by the presence of carbonate and pyrite. Cooper Basin shale reactions with water at 75 °C under slightly oxic atmospheric pressure conditions were reported previously by our group (Pearce et al., 2018b). Sphalerite oxidation was observed in a Roseneath Shale reaction resulting in a pH 3 fluid. The corrosion of siderite was observed, with precipitation of Fe-oxides and sulphides. In a Murteree Shale and water reaction, ankerite dissolution buffered pH, with Fe-oxide precipitation. The release of metals Cr, Co, Ni, Cu, Zn, Cd, and U were higher from the Roseneath Shale than the Murteree but all were < 10% of the shale total metal content.

In the current experiments, the proportion of mobilised U was

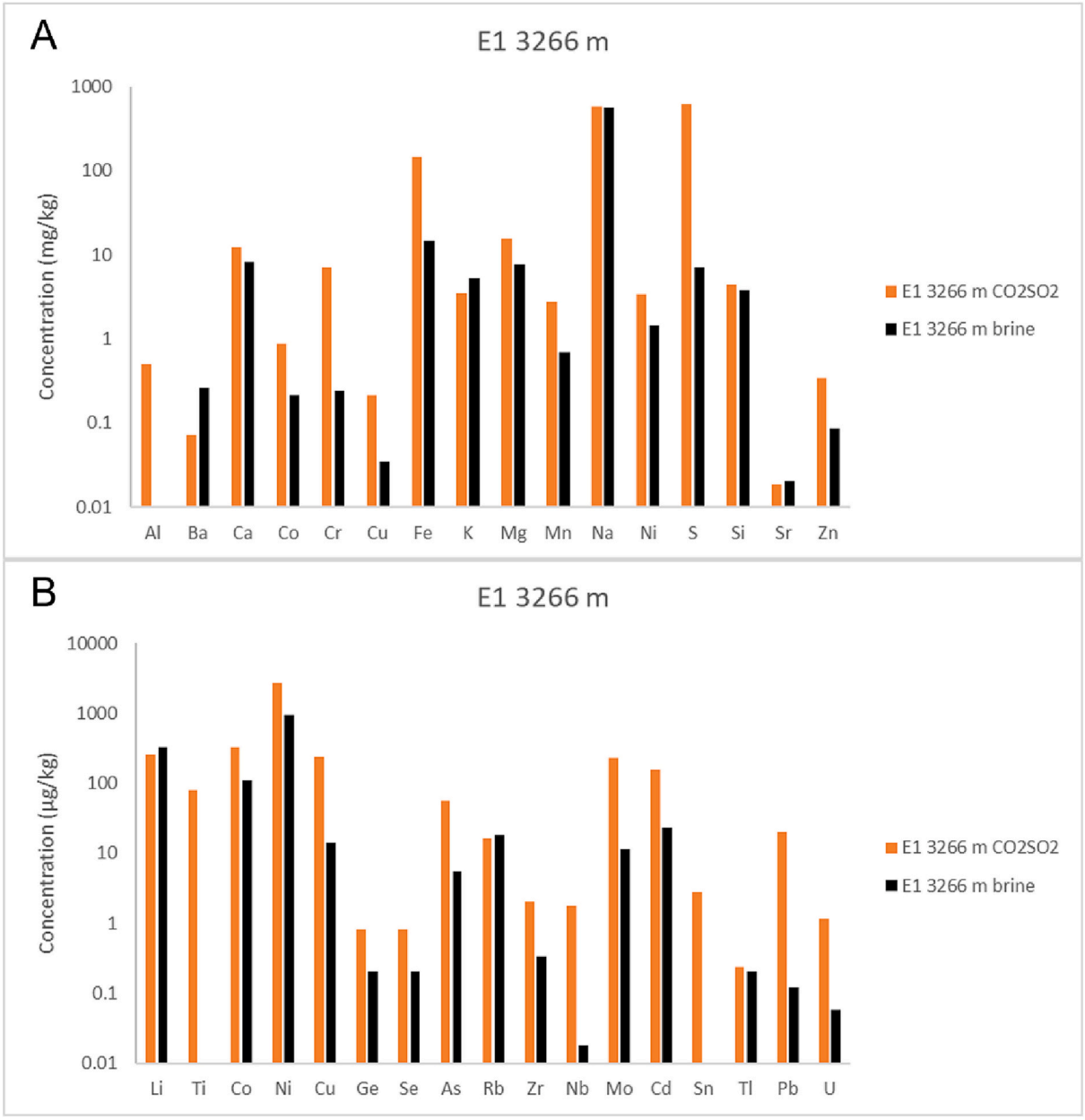

Fig. 12. Concentrations of dissolved ions released in reactions of Roseneath Shale E1 3266 m with CO_2SO_2 and brine, or with N_2 and brine. All batch experiments were at 100 °C and 20 MPa. A) Major cations (mg/kg), B) minor and trace ions (µg/kg). Note this is shown on a log scale. Na is mainly from the brine, and in the CO_2SO_2 reaction dissolved S shown here has also been sourced from the dissolved SO_2.

highest in Epsilon Formation HCl reaction, from reaction of monazite identified in the Epsilon Formation sample (supplementary material). The highest Li, K, and Si concentrations were also released in the Epsilon Formation HCl reaction owing to the lower carbonate content and less initial pH buffering resulting in higher silicate dissolution.

Comparing the CO_2SO_2 reactions of the three shales, the Roseneath Shale reaction resulted in the lowest pH at 1.23 than the other shales (pH 2.51, 2.55), with the highest dissolved sulphate concentration. The Roseneath sample was observed to contain areas of high surface area pyrite cements associated with siderite in the rock matrix. The low pH in Roseneath experiments indicates a contribution of sulphide mineral reaction releasing additional S in the Roseneath Shale reaction. Pyrite, anhydrite and barite were precipitated in shale CO_2SO_2 reactions where a portion of S, Fe, Ca and Ba were sequestered in the precipitated minerals. In the CO_2SO_2 reactions of the three shales, Pb, Cd, Cu, and Li were mobilised to solution at the highest concentrations from the Roseneath Shale. The Roseneath Shale contained the highest Pb, Cu, and Li content of the three shales, with Pb mainly in pyrite and sphalerite associated with organic matter (and siderite), and the Cu hosted in the sphalerite and chalcopyrite. The source of Li was not determined but may have included reaction of muscovite at the low generated pH and also ion exchange from clays during all reactions.

Again comparing the CO_2SO_2 shale reactions, As and Mo were released in higher concentrations from the Epsilon Formation, although the As and Mo content of the three shales was similar. In the Roseneath Shale, As was hosted in sphalerite in the organic matter. However in the Epsilon Formation and Murteree shale sphalerite was in the rock matrix and hosted Zn, but not As. In both Epsilon and Murteree samples, As tended to be hosted with Ni. In the Murteree As and Ni were associated with organic matter, however the signatures were diffuse in the organic matter poor Epsilon and may indicate that As was adsorbed to clay surfaces and desorbed during reaction.

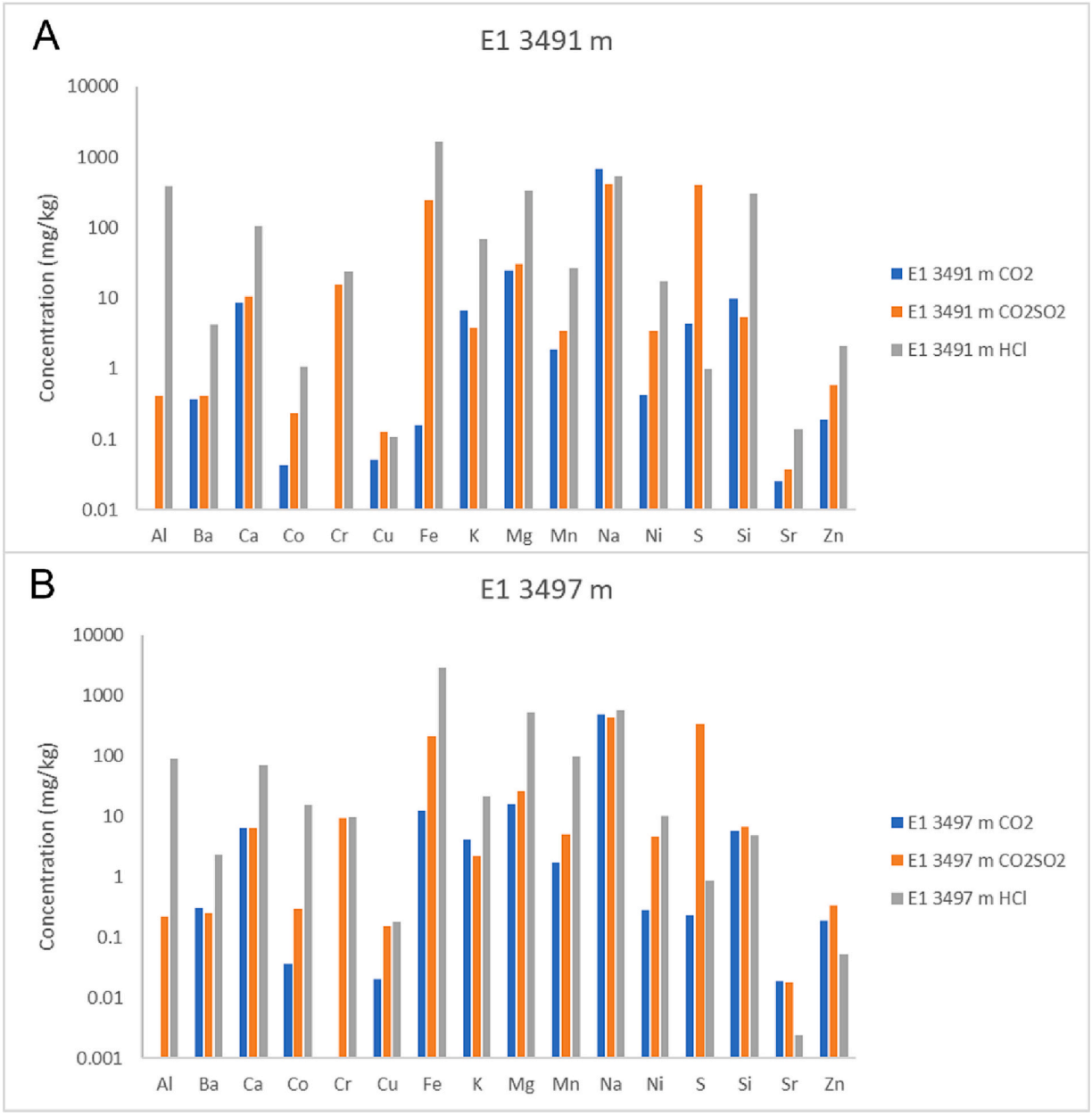

Fig. 13. Major cations (mg/kg) released in reactions with pure supercritical CO_2 and brine, with CO_2SO_2 and brine, or dilute HCl. All batch experiments were at 100 °C and 20 MPa. A) Epsilon Formation E1 3491 m and B) Murteree Shale E1 3497 m. Note this is shown on a log scale. Na is mainly from the brine, and in the CO_2SO_2 reaction dissolved S shown here has also been sourced from the dissolved SO_2.

In the pure CO_2 reactions Fe-oxides were precipitated, especially after the Epsilon Formation reaction where a higher pH was generated. The Fe-rich precipitates were spread over the shale surfaces as a thin layer or grain coating, but also concentrated on the corroded siderite in the case of the Epsilon Formation. Precipitating Fe-oxides are known to incorporate metals in their structure and also adsorb metals and elements such as As to their surfaces (Rossi et al., 2022; Shao et al., 2014; Viswanathan et al., 2012; Wigley et al., 2012). Mobilised metal concentrations were lowest after the brine reaction of the Roseneath Shale where the pH was buffered and metals were precipitated in Fe-oxides including Cr and Ni, and in precipitated barite. CO_2 based fluids may produce cleaner flow back or produced water than HCl based fluids.

3.6. Application, advantages, and limitations

The results of this study indicate that in siderite rich shales, such as those of the Cooper Basin REM, CO_2 based fracture fluids may result in cleaner production waters than HCl based fluid, however reactions may result in closing of some small pores affecting gas flow. In countries like Australia (and China) where water resources can be scarce, the use of CO_2 based fluids will be advantageous to preserve precious water resources. The avoidance of water-based fracturing fluids may also be preferable in clay rich shales such as the Cooper Basin REM, to avoid clay swelling from water. This study shows that metals are released from gas shales and that their concentrations and identities depend on the injection fluid. The release of metals from shale stimulation into formation water or produced water is an environmental and social concern if waters were to migrate or leak to overlying aquifers or get released into rivers and soils (Bondu et al., 2021; Gregory et al., 2011). Understanding the metals released is also useful where groundwaters may be monitored, or where production waters are treated, or reused for fracturing or CO_2 mineralisation (Paukert Vankeuren et al., 2017; Pearce

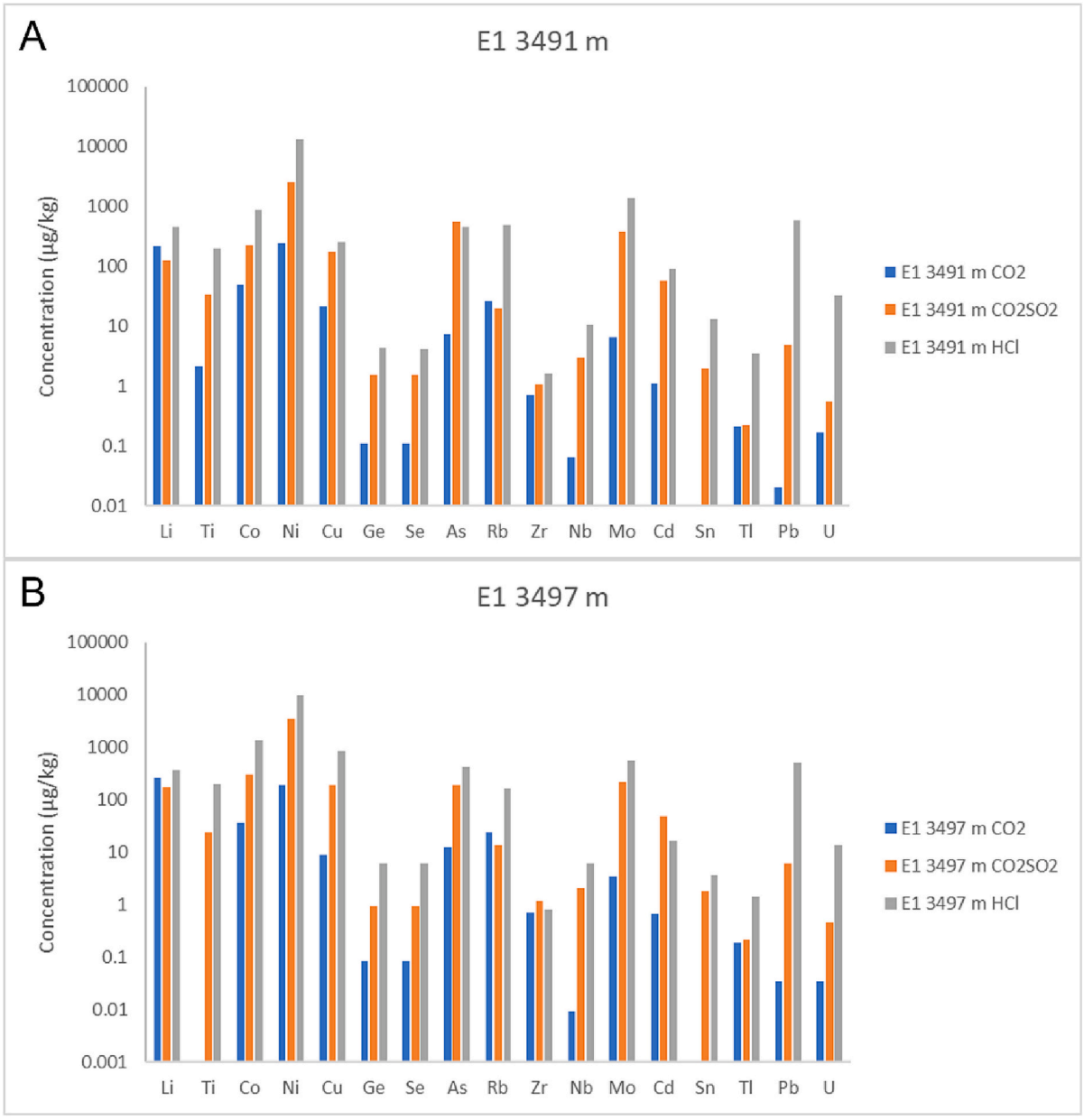

Fig. 14. Minor and trace dissolved elements and metals (µg/kg) released to solution in reactions with pure supercritical CO_2 and brine, CO_2SO_2 and brine, or dilute HCl. All batch experiments were at 100 °C and 20 MPa. A) Epsilon Formation E1 3491 m, B) Murteree Shale E1 3497 m. Note this is shown on a log scale.

Table 5
The element release at the end of experiments as a percentage of the total element available in the rock (%). All batch experiments were at 100 °C and 20 MPa. The dilute HCl experiments were pressurized with N_2, and CO_2 and CO_2SO_2 experiments also contained brine.

	E1 3491 CO_2	E1 3491 CO_2SO_2	E1 3491 HCl	E1 3497 CO_2	E1 3497 CO_2SO_2	E1 3497 HCl	E1 3266 CO_2SO_2	E1 3266 Brine
	Epsilon	Epsilon	Epsilon	Murteree	Murteree	Murteree	Roseneath	Roseneath
As	0.26	22.53	20.83	0.51	8.95	18.35	3.67	0.34
Pb	0.00	0.13	17.29	0.00	0.15	11.70	0.04	0.00
Li	4.84	3.34	13.25	5.99	4.49	9.05	3.38	4.18
Ba	0.66	0.84	9.54	0.53	0.50	4.23	0.10	0.35
U	0.02	0.07	4.52	0.00	0.06	1.74	0.14	0.01
Zn	1.98	7.10	28.41	1.77	3.70	0.54	1.80	0.44
Sr	0.44	0.77	3.09	0.38	0.42	0.05	0.40	0.42
Se	0.01	0.19	0.57	0.01	0.13	0.79	0.05	0.01
Cu	0.24	2.33	3.74	0.11	2.60	11.12	1.61	0.09

et al., 2022e; Phan et al., 2015; Phan et al., 2018; Zhu et al., 2022). However, this is an experimental laboratory study representing short term reactions. At the field scale in the actual reservoir reactions induced by fracture fluids or CO_2 can be slower and fluid:rock ratios are generally much lower (Li et al., 2008; Maskell et al., 2018; Navarre-Sitchler et al., 2013). Reactive surface areas of minerals in the reservoir, or reactive fluid accessibility to the mineral surface, can vary substantially from the laboratory, especially if crushed or powdered samples are used (Kirste et al., 2017; Kirste et al., 2019; Liu et al., 2022; Pearce et al., 2015a; Qin and Beckingham, 2021). The use of laboratory experiments to validate geochemical models, and the use of geochemical models to scale up and history match field injection tests is a way to advance the understanding of the differences of scale, and improve future predictions. In addition for CO_2 storage, an understanding of natural analogue sites of natural CO_2 storage or leakage will improve our predictions for future field injection sites for CO_2 storage, along with those for geological storage of CH_4, compressed air or H_2 (Bickle et al., 2013; Ming et al., 2016; Pearce et al., 2021c; Roberts et al., 2019; Stalker et al., 2022).

This study has also shown the different effects of different reaction fluids – acid, pure supercritical CO_2 and brine or impure CO_2 and brine, on the opening and closing of meso-pores. Accessible porosity in shale is important in shale gas extraction to allow the gas to flow out and be produced, where we observed that dilute HCl increases the number of open pores in the larger size range investigated. During CO_2 storage, maintaining accessible porosity in the reservoir near well bore is advantageous to maintain injectivity. Conversely, decreasing accessible porosity or permeability at the reservoir - cap-rock interface or in the far field is preferable to reduce CO_2 migration out of the storage complex and to increase trapping. We observed a small decrease in the accessible porosity of the shales after pure and impure CO_2 reactions. This process would be favourable if it occurs in the subsurface in the far field, however the changes may be shale mineral specific as the effect appeared to be owing to Fe-oxide, sulphate and barite precipitation where the Fe was mainly sourced from the siderite and chlorite present in the REM shales. Over longer time scales the dissolved Fe may be converted into siderite, ankerite or dolomite mineral trapping CO_2, longer experiments and geochemical predictions at near and far field conditions could be performed in future to understand these effects, along with field injection trials.

The small number of shales characterised and reacted here from the Cooper Basin Encounter 1 well is a limitation of the work. A wider range of shale samples to represent the formation heterogeneity over a wider range of depths, facies and wells could be reacted in future. In addition, the response of other Australian shale types e.g. pyrite rich or calcite rich shales to CO_2 reactions, across lacustrine vs marine, and oil vs gas shales could be investigated. Further studies should also include other fracture fluid constituents that are expected to be used locally for Australian shales, and also assess organic components that may be released to solution (Marcon et al., 2017). The experiments here were run for very short periods, longer CO_2-water-shale reactions could be performed especially for an improved understanding of long term shale reactions during CO_2 storage. Running experiments over several months with periodic collection of fluids and subsequent geochemical modelling of the data for long term predictions is suggested to understand, for example, the mineral trapping potential and storage suitability of different shale types (Pearce et al., 2019b). The water:rock ratio, temperature, and pressure conditions could also be varied to suit subsurface in situ reservoir conditions, or to investigate differences if injected CO_2 cooled the reservoir.

An improved understanding of Australian shale – fluid reactions is needed over a range of fluid, gas and shale types and mineral contents. A difference in pore size distributions with mineral content i.e. quartz-rich vs clay-rich vs carbonate rich was observed in shale from the USA, that indicates potential different effects on accessible porosity with shale type (Bahadur et al., 2018). Differences in microstructure across different USA shale formation samples has also been reported (Curtis et al., 2010). An improved understanding of the macro-porosity and pore accessibility changes across a range of Australian shales with different simulation fluids and supercritical CO_2 conditions is needed in future (Chukwuma et al., 2023). Chinese shale was shown to undergo changes in geomechanical properties after CO_2 reaction recently, with calcite dissolution, mineral precipitation and increased macro pore and crack generation (Zhou et al., 2022a; Zou et al., 2018). Therefore, Australian shale gas-water-rock reaction studies in future should also be coupled with gas and fluid permeability and geomechanical studies to understand alterations from the lab to field scale. Modelling longer term shale reactions and potential mineral trapping and metal sequestration is also recommended (Pearce et al., 2022a). In addition, an assessment of shale metals and Sr and Li isotope tracers of the shale, the formation waters, and those released to solution in reactions is needed for a range of Australian oil and gas shales, to understand if these isotope tracers will be a useful field tracer of potential surface water or groundwater contamination from shale gas or oil production (Akob et al., 2016; Chapman et al., 2012; Humez et al., 2013; Shand et al., 2009).

4. Conclusions

- Cooper Basin REM shales were characterised and reacted with dilute HCl or supercritical CO_2 or CO_2-SO_2. In XFM of the rock surfaces, As and Ni were mainly associated with sulphides in organic matter pores. Pb was mainly associated with pyrite cements, and Mn (and Cr) with siderite. Reactions of carbonates such as siderite, ankerite, and sulphides could potentially release regulated metals to production water.
- Siderite and ankerite dissolved in dilute HCl reactions, leaving pits on surfaces. Siderite/ankerite mainly reacted in in shale - formation water - CO_2 reactions with Fe-rich precipitates subsequently formed.
- In general the concentrations of metals released to solution from reaction with HCl > CO_2-SO_2 > CO_2 > N_2 and brine. Around 0 to 17% Pb, 0.3 to 23% As, 3 to 13% Li, and 0.4 to 28% Zn was released to solution as a percentage of the total available element in the shale.
- The fraction of SANS gas (CD_4) accessible mesopores was higher in the Epsilon Formation core than the Murteree and Roseneath shale samples. After CO_2 or CO_2-SO_2 reaction a small decrease in pore accessibility was more pronounced in the Murteree and Roseneath shales, consistent with mineral precipitation. Reaction with dilute HCl opened mesopores especially at ~150 nm, however those ~10 nm closed.
- Geochemical reactions during CO_2 storage in siderite rich shales may cause mesopore self-sealing, that can be favourable to avoid migration out of the storage complex. Dilute HCl reaction during acid stimulation conversely may open larger methane accessible pores. This can be favourable for the release of gas during production. Metals can be mobilised from carbonates and sulphide minerals, this may be more of an issue for HCl treatment than CO_2 based fracturing, enhanced recovery, or CO_2 storage. Mineral precipitation of Fe-oxides, barite, and pyrite in CO_2 and CO_2-SO_2 reactions also removed metals from solution including Ba, Fe, Cr and Ni.
- Understanding the mineral sources of metals in different lithology shales, and their potential release with different fracture fluids may result in better predictions and mitigation options for metal mobilisation in production water, to protect the environment. Reactions of shale samples of different lithologies and mineralogies (calcite cemented, clay rich etc.) from different locations, and comparing Australian marine and terrestrial shales is needed in future. Comparisons of experimental results with field sampled production water analysis of mobilised metals is also needed in future to enable predictive geochemical models for CO_2 storage in shales, or enhanced recovery.

CRediT authorship contribution statement

J.K. Pearce: Conceptualization, Methodology, Formal analysis, Investigation, Visualization, Writing – original draft, Visualization, Funding acquisition, Project administration. **T. Blach:** Conceptualization, Investigation, Formal analysis, Visualization, Writing – review & editing, Funding acquisition. **G.K.W. Dawson:** Formal analysis, Visualization, Validation, Investigation, Writing – review & editing. **G. Southam:** Visualization, Investigation, Formal analysis, Writing – review & editing, Funding acquisition. **D.J. Paterson:** Visualization, Investigation, Formal analysis, Writing – review & editing. **S.D. Golding:** Conceptualization, Formal analysis, Writing – review & editing, Supervision, Funding acquisition. **J. Bahadur:** Visualization, Investigation, Formal analysis. **Y.B. Melnichenko:** Visualization, Investigation, Formal analysis. **V. Rudolph:** Investigation, Formal analysis, Writing – review & editing, Supervision.

Declaration of Competing Interest

The authors declare no known competing interests.

The funding bodies had no influence in the study design; in the collection, analysis, and interpretation of data; in the writing of the paper; and in the decision to submit the paper for publication.

Data availability

Data are in the supplementary material or will be shared on request.

Acknowledgments

Luc Turner, Dean Biddle, and Lei Ge are thanked for assistance with experiments and characterisation. Part of this work was funded by a UQ CEIF Firstlink grant. The UQ SEES Environmental Geochemistry Laboratory (EGL) is thanked for assistance with analyses. The research at Oak Ridge National Laboratory's High Flux Isotope Reactor was sponsored by the Laboratory Directed Research and Development Program and the Scientific User Facilities Division, Office of Basic Energy Sciences, U.S. Department of Energy, grant IPTS-10582. Part of this research was undertaken on the XFM beamline at the Australian Synchrotron, ANSTO. This relates to grant no. AS193/XFM/15296 "Regulated metals in oil and gas shale and associated flow back fluids". We acknowledge travel funding provided by the International Synchrotron Access Program (ISAP) managed by the Australian Synchrotron, part of ANSTO, and funded by the Australian Government. Daryl Howard and Martin de Jonge are thanked for assistance at the XFM beamline. The authors acknowledge the facilities, and the scientific and technical assistance, of the Australian Microscopy & Microanalysis Research Facility at the Centre for Microscopy and Microanalysis, The University of Queensland. The anonymous reviewers and editors are thanked for their comments that have improved this manuscript.

Appendix A. Supplementary data

Supplementary data to this article can be found online at https://doi.org/10.1016/j.coal.2023.104271.

References

Akob, D.M., Mumford, A.C., Orem, W., Engle, M.A., Klinges, J.G., Kent, D.B., Cozzarelli, I.M., 2016. Wastewater Disposal from Unconventional Oil and Gas Development Degrades Stream Quality at a West Virginia Injection Facility. Environ. Sci. Technol. 50, 5517–5525.

Annevelink, M.P.J.A., Meesters, J.A.J., Hendriks, A.J., 2016. Environmental contamination due to shale gas development. Sci. Total Environ. 550, 431–438.

Armad, M., 2014. Petrophysical and Mineralogical Evaluation of Shale Gas Reservoirs (a Cooper Basin Study). University of Adelaide, Thesis.

Bachu, S., Nordbotten, J.M., Celia, M.A., 2005. Evaluation of the spread of acid-gas plumes injected in deep saline aquifers in western Canada as an analogue for CO2 injection into continental sedimentary basins. In: Rubin, E.S., Keith, D.W., Gilboy, C. F., Wilson, M., Morris, T., Gale, J., Thambimuthu, K. (Eds.), Greenhouse Gas Control Technologies 7. Elsevier Science Ltd, Oxford, pp. 479–487.

Bahadur, J., Radlinski, A.P., Melnichenko, Y.B., Mastalerz, M., Schimmelmann, A., 2015. Small-Angle and Ultrasmall-Angle Neutron Scattering (SANS/USANS) study of New Albany Shale: a Treatise on Microporosity. Energy Fuel 29, 567–576.

Bahadur, J., Ruppert, L.F., Pipich, V., Sakurovs, R., Melnichenko, Y.B., 2018. Porosity of the Marcellus Shale: a contrast matching small-angle neutron scattering study. Int. J. Coal Geol. 188, 156–164.

Barakat, S., Cook, B., D'Amore, K., Diaz, A., Bracho, A., 2019. An Australian first initiative to re-develop the first commercial onshore oilfield into a CO2 miscible-EOR project. APPEA J. 59, 179–195.

Baublys, K.A., Hamilton, S.K., Golding, S.D., Vink, S., Esterle, J., 2015. Microbial controls on the origin and evolution of coal seam gases and production waters of the Walloon Subgroup; Surat Basin, Australia. Int. J. Coal Geol. 147-148, 85–104.

BeachEnergy, 2011. Encounter - 1 Well completion report, PEL 218, South Australia.

Bickle, M.J., Kampman, N., Wigley, M., 2013. Natural analogues, Geochemistry of Geologic Carbon Sequestration, Chapter in Reviews in Mineralogy and Geochemistry, pp. 15–71.

Bondu, R., Kloppmann, W., Naumenko-Dèzes, M.O., Humez, P., Mayer, B., 2021. Potential impacts of shale gas development on inorganic groundwater chemistry: implications for environmental baseline assessment in shallow aquifers. Environ. Sci. 55 (14), 9657–9671.

Bratcher, J.C., Kaszuba, J.P., Herz-Thyhsen, R.J., Dewey, J.C., 2021. Ionic Strength and pH Effects on Water–Rock Interaction in an Unconventional Siliceous Reservoir: On the Use of Formation Water in Hydraulic Fracturing. Energy Fuel 35, 18414–18429.

Busch, A., Alles, S., Gensterblum, Y., Prinz, D., Dewhurst, D.N., Raven, M.D., Stanjek, H., Krooss, B.M., 2008. Carbon dioxide storage potential of shales. Int. J. Greenh. Gas Control 2, 297–308.

Chapman, E.C., Capo, R.C., Stewart, B.W., Kirby, C.S., Hammack, R.W., Schroeder, K.T., Edenborn, H.M., 2012. Geochemical and Strontium Isotope Characterization of Produced Waters from Marcellus Shale Natural Gas Extraction. Environ. Sci. Technol. 46, 3545–3553.

Chopping, C., Kaszuba, J.P., 2017. Reactivity of supercritical sulfur dioxide and carbon dioxide in a carbonate reservoir: an experimental investigation of supercritical fluid-brine-rock interactions relevant to the Madison Limestone of Southwest Wyoming. Interpretation 5, SS43–SS58.

Chukwuma, K., Tsikos, H., Horsfield, B., Schulz, H.-M., Harris, N.B., Frazenburg, M., 2023. The effects of Jurassic igneous intrusions on the generation and retention of gas shale in the lower Permian source-reservoir shales of Karoo Basin, South Africa. Int. J. Coal Geol. 269, 104219.

Cui, G., Yang, L., Fang, J., Qiu, Z., Wang, Y., Ren, S., 2021. Geochemical reactions and their influence on petrophysical properties of ultra-low permeability oil reservoirs during water and CO2 flooding. J. Pet. Sci. Eng. 203, 108672.

Curtis, M.E., Ambrose, R.J., Sondergeld, C.H., 2010. Structural Characterization of Gas Shales on the Micro- and Nano-Scales. Soc. Petrol. Eng. https://doi.org/10.2118/137693-ms.

Edgin, M.G., Medina-Rodriguez, B., Kaszuba, J.P., Dewey, J.C., Alvarado, V., 2021. Geochemical reactions and alteration of pore architecture in saturated shale after injection of stimulation fluid. Fuel 303, 120815.

Ellis, B., Fitts, J., Bromhal, G., McIntyre, D., Tappero, R., Peters, C., 2013. Dissolution-Driven Permeability Reduction of a Fractured Carbonate Caprock. Environ. Eng. Sci. 30, 187–193.

Farquhar, S.M., Pearce, J.K., Dawson, G.K.W., Golab, A., Kirste, D., Biddle, D., Golding, S. D., 2015. A fresh approach to investigating CO2 storage: Experimental CO2-water-rock interactions in a freshwater reservoir system. Chem. Geol. 399, 98–122.

Forde, O.N., Cahill, A.G., Mayer, K.U., Mayer, B., Simister, R.L., Finke, N., Crowe, S.A., Cherry, J.A., Parker, B.L., 2019. Hydro-biogeochemical impacts of fugitive methane on a shallow unconfined aquifer. Sci. Total Environ. 690, 1342–1354.

GA, 2017. Scientific Inquiry into Hydraulic Fracturing in the Northern Territory. https://frackinginquiry.nt.gov.au/?a=434887.

Granger, T., 2013. Mechnaisms for Anomalous Organic Matter Concentrations within the Roseneath-Epsilon-Murteree Section of the Cooper Basin. Thesis. University of Adelaide.

Gregory, K.B., Vidic, R.D., Dzombak, D.A., 2011. Water Management challenges Associated with the production of Shale Gas by Hydraulic Fracturing. Elements 7, 181–186.

Hall, L., 2015. Cooper Basin Regional Petroleum Prospectivity Studies, Regional Prospectivity Studies. Roundtable for Oil and Gas Projects in SA, Adelaide, Sept 2015.

Harrison, A.L., Jew, A.D., Dustin, M.K., Thomas, D.L., Joe-Wong, C.M., Bargar, J.R., Johnson, N., Brown Jr., G.E., Maher, K., 2017. Element release and reaction-induced porosity alteration during shale-hydraulic fracturing fluid interactions. Appl. Geochem. 82, 47–62.

Howard, D.L., de Jonge, M.D., Afshar, N., Ryan, C.G., Kirkham, R., Reinhardt, J., Kewish, C.M., McKinlay, J., Walsh, A., Divitcos, J., Basten, N., Adamson, L., Fiala, T., Sammut, L., Paterson, D.J., 2020. The XFM beamline at the Australian Synchrotron. J. Synchrotron Radiat. 27, 1447–1458.

Humez, P., Lagneau, V., Lions, J., Negrel, P., 2013. Assessing the potential consequences of CO2 leakage to freshwater resources: a batch-reaction experiment towards an isotopic tracing tool. Appl. Geochem. 30, 178–190.

İnan, S., Al Badairy, H., İnan, T., Al Zahrani, A., 2018. Formation and occurrence of organic matter-hosted porosity in shales. Int. J. Coal Geol. 199, 39–51.

Jadoon, Q.K., Roberts, E., Blenkinsop, T., Wust, R., 2016a. Organic petrography and thermal maturity of the Permian Roseneath and Murteree shales in the Cooper Basin, Australia. Int. J. Coal Geol. 154–155, 240–256.

Jadoon, Q.K., Roberts, E., Blenkinsop, T., Wust, R.A.J., Shah, S.A., 2016b. Mineralogical modelling and petrophysical parameters in Permian gas shales from the Roseneath and Murteree formations, Cooper Basin, Australia. Pet. Explor. Dev. 43, 277–284.
Jarrett, A.J.M., Munson, T.J., Williams, B., Bailey, A.H.E., Palu, T., 2022. Petroleum supersystems in the greater McArthur Basin, Northern Territory, Australia: prospectivity of the world's oldest stacked systems with emphasis on the McArthur Supersystem. APPEA J. 62, 245–262.
Jew, A.D., Dustin, M.K., Harrison, A.L., Joe-Wong, C.M., Thomas, D.L., Maher, K., Brown, G.E., Bargar, J.R., 2017. Impact of Organics and Carbonates on the Oxidation and Precipitation of Iron during Hydraulic Fracturing of Shale. Energy Fuel 31, 3643–3658.
Johnson, J.D., Graney, J.R., 2015. Fingerprinting Marcellus Shale waste products from Pb isotope and trace metal perspectives. Appl. Geochem. 60, 104–115.
Kalinowski, A., Tenthorey, E., Seyyedi, M., Clennell, M.B., 2022. The search for new oil and CO2 storage resources: residual oil zones in Australia. APPEA J. 62, 281–293.
Kirste, D., Pearce, J., Golding, S., 2017. Parameterizing Geochemical Models: do Kinetics of Calcite Matter? Proced. Earth Planet. Sci. 17, 606–609.
Kirste, D., Pearce, J.K., Golding, S.D., Dawson, G.K.W., 2019. Trace element mobility during CO2 storage: application of reactive transport modelling. E3S Web. Conf. 98, 04007.
Lacey, D.A., Zukowski, K.J., Owen, J.G., MacDonald, T.S., 2022. Techno-economic evaluation of blue hydrogen production with carbon capture and storage for onshore Eastern Australia. APPEA J. 62, S142–S148.
Li, L., Steefel, C.I., Yang, L., 2008. Scale dependence of mineral dissolution rates within single pores and fractures. Geochim. Cosmochim. Acta 72, 360–377.
Liu, D., Li, Y., Agarwal, R.K., 2016. Numerical simulation of long-term storage of CO2 in Yanchang shale reservoir of the Ordos basin in China. Chem. Geol. 440, 288–305.
Liu, X., Tournassat, C., Grangeon, S., Kalinichev, A.G., Takahashi, Y., Marques Fernandes, M., 2022. Molecular-level understanding of metal ion retention in clay-rich materials. Nat. Rev. Earth & Environ. 3, 461–476.
Mao, X., Rodrigues, S., Esterle, J.S., Golding, S.D., 2023. Reservoir lithofacies study of the Toolebuc Formation, Eromanga Basin, Australia as a potential unconventional target. Int. J. Coal Geol. 265, 104163.
Marcon, V., Kaszuba, J.P., 2015. Carbon dioxide–brine–rock interactions in a carbonate reservoir capped by shale: Experimental insights regarding the evolution of trace metals. Geochim. Cosmochim. Acta 168, 22–42.
Marcon, V., Joseph, C., Carter, K.E., Hedges, S.W., Lopano, C.L., Guthrie, G.D., Hakala, J. A., 2017. Experimental insights into geochemical changes in hydraulically fractured Marcellus Shale. Appl. Geochem. 76, 36–50.
Maskell, A., Scott, P.M., Buisman, I., Bickle, M., 2018. A siltstone reaction front related to CO2- and sulfur-bearing fluids: Integrating quantitative elemental mapping with reactive transport modeling. Am. Mineral. 103, 314–323.
Melnichenko, Y.B., He, L., Sakurovs, R., Kholodenko, A.L., Blach, T., Mastalerz, M., Radliński, A.P., Cheng, G., Mildner, D.F.R., 2012. Accessibility of pores in coal to methane and carbon dioxide. Fuel 91, 200–208.
Ming, X.R., Liu, L., Yu, M., Bai, H.G., Yu, L., Peng, X.L., Yang, T.H., 2016. Bleached mudstone, iron concretions, and calcite veins: a natural analogue for the effects of reducing CO2-bearing fluids on migration and mineralization of iron, sealing properties, and composition of mudstone cap rocks. Geofluids 16, 1017–1042.
Mouzakis, K.M., Navarre-Sitchler, A.K., Rother, G., Bañuelos, J.L., Wang, X., Kaszuba, J. P., Heath, J.E., Miller, Q.R.S., Alvarado, V., McCray, J.E., 2016. Experimental Study of Porosity changes in Shale Caprocks Exposed to CO2-Saturated Brines I: Evolution of Mineralogy, Pore Connectivity, Pore size distribution, and Surface Area. Environ. Eng. Sci. 33, 725–735.
Navarre-Sitchler, A.K., Cole, D.R., Rother, G., Jin, L., Buss, H.L., Brantley, S.L., 2013. Porosity and surface area evolution during weathering of two igneous rocks. Geochim. Cosmochim. Acta 109, 400–413.
Olmstead, S.M., Muehlenbachs, L.A., Shih, J.-S., Chu, Z., Krupnick, A.J., 2013. Shale gas development impacts on surface water quality in Pennsylvania. Proc. Natl. Acad. Sci. 110, 4962–4967.
Osborn, S.G., Vengosh, A., Warner, N.R., Jackson, R.B., 2011. Methane contamination of drinking water accompanying gas-well drilling and hydraulic fracturing. Proc. Natl. Acad. Sci. U. S. A. 108, 8172–8176.
Paterson, D., Jonge, M.D.D., Howard, D.L., Lewis, W., McKinlay, J., Starritt, A., Kusel, M., Ryan, C.G., Kirkham, R., Moorhead, G., Siddons, D.P., 2011. The X-ray Fluorescence Microscopy Beamline at the Australian Synchrotron. In: AIP Conference Proceedings, 1365, pp. 219–222.
Paukert Vankeuren, A.N., Hakala, J.A., Jarvis, K., Moore, J.E., 2017. Mineral Reactions in Shale Gas Reservoirs: Barite Scale Formation from Reusing Produced Water as Hydraulic Fracturing Fluid. Environ. Sci. Technol. 51, 9391–9402.
Pearce, J.K., Kirste, D.M., Dawson, G.K.W., Farquhar, S.M., Biddle, D., Golding, S., Rudolph, V., 2015a. SO2 Impurity Impacts on Experimental and simulated CO2-Water-Reservoir Rock Reactions at Carbon Storage Conditions. Chem. Geol. 399, 65–86.
Pearce, J.K., Law, A.C.K., Dawson, G.K.W., Golding, S.D., 2015b. SO2-CO2 and pure CO2 reactivity of ferroan carbonates at carbon storage conditions. Chem. Geol. https://doi.org/10.1016/j.chemgeo.2015.07.001.
Pearce, J.K., Dawson, G.K.W., Blach, T.P., Bahadur, J., Melnichenko, Y.B., Golding, S.D., 2018a. Impure CO2 reaction of feldspar, clay, and organic matter rich cap-rocks: Decreases in the fraction of accessible mesopores measured by SANS. Int. J. Coal Geol. 185, 79–90.
Pearce, J.K., Turner, L., Pandey, D., 2018b. Experimental and predicted geochemical shale-water reactions: Roseneath and Murteree shales of the Cooper Basin. Int. J. Coal Geol. 187, 30–44.
Pearce, J.K., Dawson, G.K.W., Golab, A., Knuefing, L., Sommacal, S., Rudolph, V., Golding, S.D., 2019a. A combined geochemical and μCT study on the CO2 reactivity of Surat Basin reservoir and cap-rock cores: Porosity changes, mineral dissolution and fines migration. Int. J. Greenh. Gas Control 80, 10–24.
Pearce, J.K., Kirste, D.M., Dawson, G.K.W., Rudolph, V., Golding, S.D., 2019b. Geochemical modelling of experimental O2–SO2–CO2 reactions of reservoir, cap-rock, and overlying cores. Appl. Geochem. 109, 104401.
Pearce, J.K., La Croix, A.D., Underschultz, J.R., Golding, S.D., 2020. Long term reactivity of CO2 in a low salinity reservoir-seal complex. Appl. Geochem. 114, 104529.
Pearce, J.K., Brink, F., Dawson, G.W., Poitras, J., Southam, G., Paterson, D.J., Wolhuter, A., Underschultz, J.R., 2021a. Core characterisation and predicted CO2 reactivity of sandstones and mudstones from an Australian oil field. Int. J. Coal Geol. 103911.
Pearce, J.K., Dawson, G.K.W., Sommacal, S., Golding, S.D., 2021b. Micro CT and Experimental Study of Carbonate Precipitation from CO2 and Produced Water CO-Injection into Sandstone. Energies 14, 6998.
Pearce, J.K., La Croix, A.D., Brink, F.J., Hayes, P.J., Underschultz, J.R., 2021c. CO2 mineral trapping comparison in different regions: predicted geochemical reactivity of the Precipice Sandstone reservoir and overlying Evergreen Formation. Pet. Geosci. 27 petgeo2020-2106.
Pearce, J., Raza, S., Baublys, K., Hayes, P., Firouzi, M., Rudolph, V., 2022a. Unconventional CO2 Storage: CO2 Mineral Trapping Predicted in Characterized Shales, Sandstones, and Coal Seam Interburden. SPE J. 1–22.
Pearce, J.K., Dawson, G.W., Golding, S.D., Southam, G., Paterson, D.J., Brink, F., Underschultz, J.R., 2022b. Predicted CO2 water rock reactions in naturally altered CO2 storage reservoir sandstones, with interbedded cemented and coaly mudstone seals. Int. J. Coal Geol. 253, 103966.
Pearce, J.K., Dawson, G.W., Southam, G., Paterson, D., Kirste, D., Golding, S.D., 2022c. Metal Mobilization from CO2 Storage Cap-Rocks: Experimental Reactions with Pure CO2 or CO2 SO2 NO. Front. Energy Res. 10.
Pearce, J.K., Golding, S.D., Baublys, K., Hofmann, H., Gargiulo, G., Herbert, S.J., Hayes, P., 2022d. Methane in aquifers and alluvium overlying a coal seam gas region: gas concentrations and isotopic differentiation. Sci. Total Environ. 160639.
Pearce, J.K., Khan, C., Golding, S.D., Rudolph, V., Underschultz, J.R., 2022e. Geological storage of CO2 and acid gases dissolved at surface in production water. J. Pet. Sci. Eng. 210, 110052.
Phan, T.T., Capo, R.C., Stewart, B.W., Graney, J.R., Johnson, J.D., Sharma, S., Toro, J., 2015. Trace metal distribution and mobility in drill cuttings and produced waters from Marcellus Shale gas extraction: Uranium, arsenic, barium. Appl. Geochem. 60, 89–103.
Phan, T.T., Paukert Vankeuren, A.N., Alexandra Hakala, J., 2018. Role of water−rock interaction in the geochemical evolution of Marcellus Shale produced waters. Int. J. Coal Geol. 191, 95–111.
Porter, R.T.J., Fairweather, M., Pourkashanian, M., Woolley, R.M., 2015. The range and level of impurities in CO2 streams from different carbon capture sources. Int. J. Greenh. Gas Control 36, 161–174.
Qin, F., Beckingham, L.E., 2021. The impact of mineral reactive surface area variation on simulated mineral reactions and reaction rates. Appl. Geochem. 124, 104852.
Renock, D., Landis, J.D., Sharma, M., 2016. Reductive weathering of black shale and release of barium during hydraulic fracturing. Appl. Geochem. 65, 73–86.
Roberts, J.J., Leplastrier, A., Feitz, A.J., Shipton, Z.K., Bell, A.F., Karolytė, R., 2019. Structural controls on the location and distribution of CO2 emission at a natural CO2 spring in Daylesford. Australia Int. J. Greenh. Gas Control 84, 36–46.
Ross, D.J.K., Bustin, R.M., 2009. The importance of shale composition and pore structure upon gas storage potential of shale gas reservoirs. Mar. Pet. Geol. 26, 916–927.
Rossi, L., Loisy, C., Cerepi, A., Petit, A., Le Roux, O., Estublier, A., Noirez, S., Martin, F., Hautefeuille, B., Brichart, T., Garcia, B., 2022. Dissolved trace elements dynamics during a rich-CO2-water leakage in a near-surface carbonate freshwater aquifer. Int. J. Greenh. Gas Control 114, 103561.
Ruppert, L.F., Sakurovs, R., Blach, T.P., He, L., Melnichenko, Y.B., Mildner, D.F.R., Alcantar-Lopez, L., 2013. A USANS/SANS study of the accessibility of pores in the Barnett shale to methane and water. Energy Fuel 27, 772–779.
Ryan, C.G., Siddons, D.P., Kirkham, R., Dunn, P.A., Kuczewski, A., Moorhead, G., De Geronimo, G., Paterson, D.J., De Jonge, M.D., Hough, R.M., Lintern, M.J., Howard, D.L., Kappen, P., Cleverley, J., 2010. The new Maia detector system: Methods for high definition trace element imaging of natural material. In: AIP Conference Proceedings, pp. 9–17.
Ryan, C.G., Siddons, D.P., Kirkham, R., Li, Z.Y., de Jonge, M.D., Paterson, D.J., Kuczewski, A., Howard, D.L., Dunn, P.A., Falkenberg, G., Boesenberg, U., De Geronimo, G., Fisher, L.A., Halfpenny, A., Lintern, M.J., Lombi, E., Dyl, K.A., Jensen, M., Moorhead, G.F., Cleverley, J.S., Hough, R.M., Godel, B., Barnes, S.J., James, S.A., Spiers, K.M., Alfeld, M., Wellenreuther, G., Vukmanovic, Z., Borg, S., 2014. Maia X-ray fluorescence imaging: Capturing detail in complex natural samples. J. Phys. Conf. Ser. 499, 012002.
Saeedi, A., Delle Piane, C., Esteban, L., Xie, Q., 2016. Flood characteristic and fluid rock interactions of a supercritical CO2, brine, rock system: South West Hub, Western Australia. Int. J. Greenh. Gas Control 54, 309–321.
Sander, R., Pan, Z., Connell, L.D., Camilleri, M., Grigore, M., Yang, Y., 2018. Controls on methane sorption capacity of Mesoproterozoic gas shales from the Beetaloo Sub-basin, Australia and global shales. Int. J. Coal Geol. 199, 65–90.
Shand, P., Darbyshire, D.P.F., Love, A.J., Edmunds, W.M., 2009. Sr isotopes in natural waters: applications to source characterisation and water–rock interaction in contrasting landscapes. Appl. Geochem. 24, 574–586.
Shao, H., Kukkadapu, R.K., Krogstad, E.J., Newburn, M.K., Cantrell, K.J., 2014. Mobilization of metals from Eau Claire siltstone and the impact of oxygen under geological carbon dioxide sequestration conditions. Geochim. Cosmochim. Acta 141, 62–82.

Smith, M.M., Sholokhova, Y., Hao, Y., Carroll, S.A., 2013. Evaporite Caprock Integrity: an Experimental Study of Reactive Mineralogy and Pore-Scale Heterogeneity during Brine-CO2 Exposure. Environ. Sci. Technol. 47, 262–268.
Snæbjörnsdóttir, S.Ó., Sigfússon, B., Marieni, C., Goldberg, D., Gislason, S.R., Oelkers, E. H., 2020. Carbon dioxide storage through mineral carbonation. Nat. Rev. Earth & Environ. 1, 90–102.
Stalker, L., Roberts, J.J., Mabon, L., Hartley, P.G., 2022. Communicating leakage risk in the hydrogen economy: Lessons already learned from geoenergy industries. Front. Energy Res. 10.
Sun, M., Yu, B., Hu, Q., Yang, R., Zhang, Y., Li, B., Melnichenko, Y.B., Cheng, G., 2018. Pore structure characterization of organic-rich Niutitang shale from China: small angle neutron scattering (SANS) study. Int. J. Coal Geol. 186, 115–125.
Talman, S., 2015. Subsurface geochemical fate and effects of impurities contained in a CO2 stream injected into a deep saline aquifer: what is known. Int. J. Greenh. Gas Control 40, 267–291.
Tanaka, K., Okawa, H., Hashimoto, K., Takahashi, R., Imai, A., Sugawara, K., 2016. Effect of NO2 in exhaust gas from an oxyfuel combustion system on the cap rock of a proposed CO2 injection site. Appl. Geochem. 70, 17–26.
Tian, H., Xu, T., Wang, F., Patil, V.V., Sun, Y., Yue, G., 2014. A numerical study of mineral alteration and self-sealing efficiency of a caprock for CO2 geological storage. Acta Geotech. 9, 87–100.
Troup, A., Edwards, S., Grigorescu, M., Dixon, O., Gopalakrishnan, S., McKillop, M., 2018. The Shale Oil Potential of the Toolebuc Formation, Eromanga and Carpentaria Queensland: Data and interpretation. Queensland Geological Record 2018/01.
Turner, L.G., Dawson, G.K.W., Golding, S.D., Pearce, J.K., 2022. CO2 and NOx reactions with CO2 storage reservoir core: NOx dissolution products and mineral reactions. Int. J. Greenh. Gas Control 120, 103750.
Viswanathan, H., Dai, Z., Lopano, C., Keating, E., Hakala, J.A., Scheckel, K.G., Zheng, L., Guthrie, G.D., Pawar, R., 2012. Developing a robust geochemical and reactive transport model to evaluate possible sources of arsenic at the CO2 sequestration natural analog site in Chimayo, New Mexico. Int. J. Greenh. Gas Control 10, 199–214.
Wang, H., Rezaee, R., 2020. CO2 Storage with Enhanced Gas Recovery CS-EGR in Conventional and Unconventional Gas Reservoirs in Australia, (SPE Asia Pacific Oil & Gas Conference and Exhibition).
Wang, L., Fortner, J.D., Giammar, D.E., 2015. Impact of Water Chemistry on Element Mobilization from Eagle Ford Shale. Environ. Eng. Sci. 32, 310–320.
Wang, L., Burns, S., Giammar, D.E., Fortner, J.D., 2016. Element mobilization from Bakken shales as a function of water chemistry. Chemosphere 149, 286–293.
Wang, K., Wang, J., Hao, J., Shi, C., Pan, S., Marathe, S., Taylor, K.G., Ma, L., 2023. Nano-scale synchrotron imaging of shale swelling in the presence of water. Fuel 344, 127999.
Wigley, M., Kampman, N., Dubacq, B., Bickle, M., 2012. Fluid-mineral reactions and trace metal mobilization in an exhumed natural CO2 reservoir, Green River, Utah. Geology 40, 555–558.
Wignall, G.D., Littrell, K.C., Heller, W.T., Melnichenko, Y.B., Bailey, K.M., Lynn, G.W., Myles, D.A., Urban, V.S., Buchanan, M.V., Selby, D.L., Butler, P.D., 2012. The 40 m general purpose small-angle neutron scattering instrument at Oak Ridge National Laboratory. J. Appl. Crystallogr. 45, 990–998.
Wilke, F.D.H., Vieth-Hillebrand, A., Naumann, R., Erzinger, J., Horsfield, B., 2015. Induced mobility of inorganic and organic solutes from black shales using water extraction: Implications for shale gas exploitation. Appl. Geochem. 63, 158–168.
Wu, W., Sharma, M.M., 2017. Acid Fracturing in Shales: effect of Dilute Acid on Properties and Pore Structure of Shale. Soc. Petrol. Eng. 32 https://doi.org/10.2118/173390-PA.
Zhang, C.P., Cheng, P., Ma, Z.Y., Ranjith, P.G., Zhou, J.P., 2021. Comparison of fracturing unconventional gas reservoirs using CO2 and water: an experimental study. J. Pet. Sci. Eng. 203, 108598.
Zhou, D., Zhang, G., Huang, Z., Zhao, J., Wang, L., Qiu, R., 2022a. Changes in microstructure and mechanical properties of shales exposed to supercritical CO2 and brine. Int. J. Rock Mech. Min. Sci. 160, 105228.
Zhou, J., Tian, S., Xian, X., Zheng, Y., Yang, K., Liu, J., 2022b. Comprehensive Review of Property Alterations Induced by CO2–Shale Interaction: Implications for CO2 Sequestration in Shale. Energy Fuel 36, 8066–8080.
Zhu, B., Wilson, S.A., Zeyen, N., Raudsepp, M.J., Zolfaghari, A., Wang, B., Rostron, B.J., Snihur, K.N., von Gunten, K., Harrison, A.L., Alessi, D.S., 2022. Unlocking the potential of hydraulic fracturing flowback and produced water for CO2 removal via mineral carbonation. Appl. Geochem. 142, 105345.
Zou, Y., Li, S., Ma, X., Zhang, S., Li, N., Chen, M., 2018. Effects of CO2–brine–rock interaction on porosity/permeability and mechanical properties during supercritical-CO2 fracturing in shale reservoirs. J. Nat. Gas Sci. Eng. 49, 157–168.